

Material Matters™

Volume 10, Number 4

ALDRICH
Materials Science



Biomaterials for Tissue Engineering

New Scaffolds for Life Science

MICRO- AND NANOFABRICATED BIOMATERIALS

FOR THE STUDY OF CELLS AND MICROTISSUES

INJECTABLE HYDROGELS

FOR CELL DELIVERY AND TISSUE REGENERATION

THREE-DIMENSIONAL PRINTING

OF TISSUE ENGINEERING SCAFFOLDS

TAILORING COLLAGEN-BASED MATRICES

FOR REGENERATIVE MEDICINE AND TISSUE ENGINEERING

SIGMA-ALDRICH®

Introduction

Welcome to the fourth issue of *Material Matters*™ 2015, focused on materials for tissue engineering and regenerative medicine. This issue highlights the use of organic and inorganic materials for elucidating cell-material interactions and for the creation of hydrogels and scaffolds for cell encapsulation, culture, and delivery.

In the first article, Professor Tejal Desai (University of California, San Francisco, USA) reviews the interface between materials science and biology, and illustrates how advances in micro- and nanotechnology using biomaterials have enhanced our understanding of cells and microtissues. Biomaterials such as fluorescent probes, inorganic nanoparticles, and polymer-based particulates can be used to make biosensors in order to quantify cell-cell, cell-matrix, and microtissue interactions.

In the second article, Professor April Kloxin (University of Delaware, USA) highlights advances in the design principles and polymer chemistries used for injectable hydrogels, including application examples in cell delivery and tissue engineering. Natural and synthetic polymeric building blocks are essential for designing injectable hydrogels that control material structural and mechanical properties, as well as the biological properties (e.g., biodegradability) of *in situ* forming hydrogels.

Professor Benjamin Wu (University of California, Los Angeles, USA), in the third article, explores the technological advances of 3D printing to create tissue engineering scaffolds. The ability to create complex 3D shapes is essential for applications in biomedical tissue engineering and regenerative medicine. The article discusses 3D printing technologies and materials, including powder 3D printing, fused-deposition molding, stereolithography, selective laser sintering, and 3D plotting/direct-wire bioprinting to make materials with controlled architectures.

In the final article, Professor Hyunjoon Kong (University of Illinois, Urbana-Champaign, USA) and Professor Liam Grover (University of Birmingham, UK) review strategies and techniques to customize collagens as building blocks for tissue engineering matrices. Modulation of the biomolecular, chemical, and mechanical characteristics of collagen by chemical conjugation and by tuning mechanical properties can improve the performance of collagen-based materials for tissue engineering and promote the restoration of tissues *in vitro* and *in vivo*.

Each article in this issue is accompanied by a list of polymers and related products available from Aldrich® Materials Science. Contact us at matsci@sial.com if you need any material that you cannot find in our catalog, or if you would like a custom grade for your development work. We welcome your new product requests and suggestions as we continue to grow our polymer offering.

About Our Cover

Biomaterials innovation is helping to expand the boundaries of life science and medical research. Polymeric and inorganic building blocks can be used to create biomaterial scaffolds for cell encapsulation, tissue engineering, and for studying cell-material interactions. The cover art for this issue artistically depicts green scaffolds interposed with images of fluorescently labeled cells and materials and yellow-orange porous hydrogel scaffolds. The inspiration for the yellow-orange porous hydrogel scaffolds is based upon poly(ethylene glycol) and poly(D,L-lactide)-based biomaterials fabricated using stereolithography in aqueous solutions of photo-crosslinkable biodegradable materials. The hydrogel scaffold image is courtesy of Tetsu Seck, Ferry Melchels, Jan Feijen, and Dirk Grijpma, Department of Biomaterials Science and Technology, University of Twente, Netherlands.



Nicolynn Davis, Ph.D.
Aldrich Materials Science

Material Matters™

Vol. 10, No. 4

**Aldrich Materials Science
Sigma-Aldrich Co. LLC**
6000 N. Teutonia Ave.
Milwaukee, WI 53209, USA

To Place Orders

Telephone 800-325-3010 (USA)
FAX 800-325-5052 (USA)

International customers, contact your local Sigma-Aldrich office (sigma-aldrich.com/worldwide-offices).

Customer & Technical Services

Customer Inquiries	800-325-3010
Technical Service	800-325-5832
SAFC®	800-244-1173
Custom Synthesis	800-244-1173
Flavors & Fragrances	800-227-4563
International	314-771-5765
24-Hour Emergency	314-776-6555
Safety Information	sigma-aldrich.com/safetycenter
Website	sigma-aldrich.com
Email	aldrich@sial.com

Subscriptions

Request your FREE subscription to *Material Matters*:

Phone	800-325-3010 (USA)
Mail	Attn: Marketing Communications Aldrich Chemical Co., Inc Sigma-Aldrich Co. LLC P.O. Box 2060 Milwaukee, WI 53201-2060
Website	aldrich.com/mm
Email	sams-usa@sial.com

Online Versions

Explore previous editions
of *Material Matters* aldrich.com/materialmatters



Available for your iPad®
aldrich.com/mm

Material Matters (ISSN 1933-9631) is a publication of Aldrich Chemical Co., Inc. Aldrich is a member of the Sigma-Aldrich Group.

©2015 Sigma-Aldrich Co. LLC. All rights reserved. SIGMA, SAFC, SIGMA-ALDRICH, ALDRICH and SUPELCO are trademarks of Sigma-Aldrich Co. LLC, registered in the US and other countries. Material Matters is a trademark of Sigma-Aldrich Co. LLC. Tetronic is a registered trademark of BASF. iPad is a registered trademark of Apple Inc. RESOMER is a registered trademark of Evonik Rohm GmbH. Sigma-Aldrich, Sigma, Aldrich, Supelco, and SAFC brand products are sold by affiliated Sigma-Aldrich distributors. Purchaser must determine the suitability of the product(s) for their particular use. Additional terms and conditions may apply. Sigma-Aldrich Corp. is a subsidiary of Merck KGaA, Darmstadt, Germany. Please see product information on the Sigma-Aldrich website at www.sigmaaldrich.com and/or on the reverse side of the invoice or packing slip.

Table of Contents

Articles

Micro- and Nanofabricated Biomaterials for the Study of Cells and Microtissues	105
Injectable Hydrogels for Cell Delivery and Tissue Regeneration	114
Three-dimensional Printing of Tissue Engineering Scaffolds	120
Tailoring Collagen-based Matrices for Regenerative Medicine and Tissue Engineering	126

Featured Products

Functionalized Gold Nanoparticles A list of gold functionalized nanomaterials	109
Gold Nano-Urchins A list of gold nano-urchins	109
Silver Nanoparticles A selection of functionalized silver nanoparticles	110
Iron Oxide A selection of functionalized iron oxide nanomaterials	110
Fluorescent Nanodiamonds A list of fluorescent nanodiamonds	110
Fluorescent Silica Nanobeads A list of fluorescent silica nanobeads	111
Preformed PLGA Biodegradable Particles A list of PLGA nanoparticles and microspheres	111
Biosensor Polymers (Stimulus-responsive Polymers) A selection of PNIPAM and polymethacrylate materials	111
Functional Polystyrene for Particle Formation and Conjugation A selection of functionalized polystyrene	113
Poly(ethylene glycol) and Poly(ethylene oxide) A selection of multi arm PEGs and copolymers, and homo- and heterofunctional PEGs	118
Synthetic Polymers for 3D Printing A selection of polycaprolactones and block PCL polymers	123
ABS 3D Printing Filaments A list of ABS filaments for 3D printing	123
PLA 3D Printing Filaments A list of PLA filaments for 3D printing	124
Biodegradable Polymers An assortment of poly(lactides)	124
High-purity Collagen A selection of bovine collagens	131
Other Natural Polymers A list of chitosan and alginate acid	131

Your Materials Matter



Bryce P. Nelson, Ph.D.
Aldrich Materials Science Initiative Lead

We welcome fresh product ideas. Do you have a material or compound you wish to see featured in the Aldrich® Materials Science line? If it is needed to accelerate your research, it matters. Send your suggestion to matsci@sial.com for consideration.

Professor John Kao at the University of Wisconsin-Madison, USA, recently recommended the addition of hydrogels for the encapsulation and controlled release of drugs, biomolecules, and cells to our catalog. We have developed two new, ready-to-use hydrogel kits that allow release of target molecules and cells in a temporally and spatially controlled manner. Hydrogels based on gelatin and poly(ethylene glycol) (PEG) combine the durability of synthetic polymers and the biorecognition of natural proteins into one delivery platform.^{1,2} Aldrich® Materials Science offers two ready-to-use hydrogel kits that can be crosslinked chemically or by photopolymerization *in situ*. These hydrogels have been used to encapsulate various cell types such as fibroblasts, keratinocytes, and mesenchymal stem cells; as well as small molecule drugs such as peptides and growth factors.^{1,3-6}

References

- (1) Fu, Y.; Xu, K.; Zheng, X.; Giacomini, A. J.; Mix, A. W.; Kao, W. J. *Biomaterials* **2012**, *33* (1), 48–58.
- (2) Xu, K.; Fu, Y.; Chung, W.; Zheng, X.; Cui, Y.; Hsu, I. C.; Kao, W. J. *Acta Biomater* **2012**, *8* (7), 2504–2516.
- (3) Guerra, A. D.; Cantu, D. A.; Vecchi, J. T.; Rose, W. E.; Hematti, P.; Kao, W. J. *AAPS J* **2015**.
- (4) Kleinbeck, K. R.; Bader, R. A.; Kao, W. J. *J Burn Care Res* **2009**, *30* (1), 98–104.
- (5) Cantu, D. A.; Hematti, P.; Kao, W. J. *Stem Cells Transl Med* **2012**, *1* (10), 740–749.
- (6) Waldeck, H.; Chung, A. S.; Kao, W. J. *J Biomed Mater Res A* **2007**, *82* (4), 861–871.

Product Description	Prod. No.
Photo-crosslinkable sIPN hydrogel kit	799610-1KT
Chemically crosslinkable sIPN hydrogel kit	799629-1KT

For more information on the availability of these kits, visit aldrich.com/ipn

MICRO- AND NANOFABRICATED BIOMATERIALS FOR THE STUDY OF CELLS AND MICROTISSUES



Phin Peng Lee, Karen E. Samy, Miquella G. Chavez, Alec Cerchiari, Tejal A. Desai*
 Department of Bioengineering and Therapeutic Sciences, University of California
 San Francisco, San Francisco, CA 94158 USA
 *Email: tejal.desai@ucsf.edu

Introduction

Biomaterials science involves the design and fabrication of smart materials for studying, directing, or mimicking biology. For successful integration of biomaterials in biological research, a meaningful understanding of biological systems is required. Furthermore, since we are at the interface of materials science and biology, advancements in the latter are often sparked by breakthroughs in the former. Accordingly, the progress in micro- and nanotechnology has significantly enhanced our understanding of cells and microtissues. Here, we discuss interesting advances in biomaterials in the context of cellular and multicellular systems.

At the Cellular Level: Fluorescent and Inorganic Probes

At the cellular level, fluorescent probes are one of the most commonly used tools for visualizing and quantifying biological events and signals. Fluorescent protein-based indicators can target subcellular compartments and be incorporated into a wider variety of tissues and intact organisms than simple organic dyes. In addition, fluorescent probes cause less photodynamic toxicity than organic dyes while still maintaining a high temporal and spatial resolution. A multitude of fluorescent probes are derived from the jellyfish *Aequorea victoria* (AFPs) including green fluorescent protein (GFP) (Roche Prod. No. 11814524001), red fluorescent protein (RFP), and cyan fluorescent protein (CFP), to name just a few. The engineering of these probes provides tools to investigate multiple

complex processes within live cells. However, rapid photobleaching and high sensitivity to chloride fluctuations and pH have driven the development of more stable AFP variants.¹ One example is coral green fluorescent protein (CGFP) which, despite its lack of brightness and broad emission and excitation peaks, is highly pH-resistant, making it ideal for use in labeling acidic cellular organelles. AFPs have been especially valuable as Fluorescence Resonance Energy Transfer (FRET)-based indicators. FRET occurs when two fluorophores are in proximity of each other (80 Å) and the emission spectrum of the donor overlaps the excitation of the acceptor. The ratio of acceptor to donor fluorescence is used as a readout for measuring biochemical events in cells. Fluorescent probes are continually being improved to provide new insights into the biology of live cells. For example, a new generation of highly sensitive near infrared fluorescent probes may be able to detect subtle conformational changes in proteins, thereby improving detection limits and applicability of AFP-based reporters.² Additionally, single-cell and single-molecule imaging can elucidate cell-to-cell variability and permits the visualization of individual molecular interactions, both of which are challenging for existing techniques.

As an alternative to fluorescent-based probes, inorganic nanoparticles, such as gold nanoparticles, iron oxide nanoparticles, and quantum dots (QDs) can be synthesized in different sizes, shapes, and yields by varying reaction times and solvents. Methods to synthesize inorganic nanoparticles include microemulsions, thermal decomposition, hydrothermal and solvothermal synthesis.³ Collectively, these particles have been used in a variety of biomedical applications including fluorescence and magnetic resonance imaging, cell targeting, and drug delivery.³ In a study on intestinal absorption, Simovic et al. characterized the physicochemical properties and *in vivo* drug delivery capabilities of nanoparticles consisting of a hydrophobic phospholipid core and a PEG hydrophilic corona (Figure 1). These PEGylated phospholipid nanoparticles can solubilize and retain water-insoluble anticancer drugs while maintaining a size distribution close to the drug-free particles.⁴ Of particular note are QDs, which have recently permeated methods in cellular and molecular biology. Composed of a semiconductor core (Cd or Se) with a shell (ZnS), the optical characteristics of QDs are drastically improved over organic fluorescent dyes. Tunable core sizes of QDs generate a wide range of narrow emission peaks and broad excitation spectra. These characteristics make QDs ideal for single-molecule tracking (SPT), fluorescence multiplexing, and FRET. The use of quantum dots in SPT has even led to new insights into the dynamics of cell surface receptors. For example, water stabilized QDs have been used to track receptor-mediated endocytic trafficking events in live cells using fluorescence microscopy.⁵ The use of QDs as FRET donors, however, is still an emerging technology. Advancements in the generation of brighter and smaller QDs will allow the development of combined SPT and FRET techniques, revolutionizing the field of membrane receptor dynamics, activation, and transport.⁵

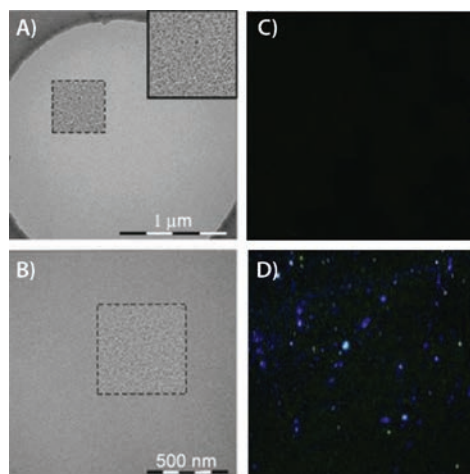


Figure 1. Transmission electron micrograph (TEM) image of PEG nanoparticles (A). Higher resolution was accomplished by band pass filtering (B). Disulfide cleaved PEG2000-SS-Biotin nanoparticles do not fluoresce with the addition of avidin-FITC (C). However, intact PEG2000-SS-Biotin particles bind avidin-FITC and are visualized via fluorescence microscopy (D). Adapted from Reference 3 with permission.

At the Cellular Level: Cellular Interactions

Beyond imaging, the advancements of smart materials and sensors facilitate the study of the physical forces between cells and their environment. Quantifying the forces involved in cell–cell and cell–matrix interactions has led to a greater understanding of the feedback of external-to-internal physical cues and their role in affecting cell behavior. Initially, Harris et al. developed a system of culturing cells on soft silicone substrates to study cell locomotion and its associated forces on the surrounding matrix.⁶ The soft substrate permits any forces exerted by the cells on the silicone to be visualized in the form of wrinkle formation on the substrate surface. Using a combination of microneedles and counterweights to re-create these wrinkles, shear forces exerted on these surfaces can be calculated.⁶

Technology for studying cellular forces is much more sophisticated today. Various forms of force microscopy now exist, allowing for a more quantitative measurement of the forces exerted by cells, either on one another or on the matrix around them. Traction Force Microscopy (TFM) is an evolution of the system developed by Harris et al. Advancements in TFM, such as the ability to analyze more than two dimensions, has opened up the possibility of studying not just the traditional shear traction in the plane of the substrate but also the inward forces exerted by the cells.⁷ As shown in **Figure 2**, Legant et al. developed a system to measure the forces exerted by cells within a three-dimensional (3D) matrix using TFM.⁷ Briefly, GFP-expressing cells were encapsulated in a PEG hydrogel (with known mechanical properties) containing fluorescent beads in the vicinity of each cell. Tracking the displacement of the beads within the surrounding matrix enabled linear elastic theory and finite element methods to be used to calculate the cellular traction forces.⁷ This powerful tool permits quantification of the cell–matrix interactions in a spatio-temporal manner, opening up many possibilities for the future study of various cell types, cell–ligand interaction studies, and even multicellular interactions.

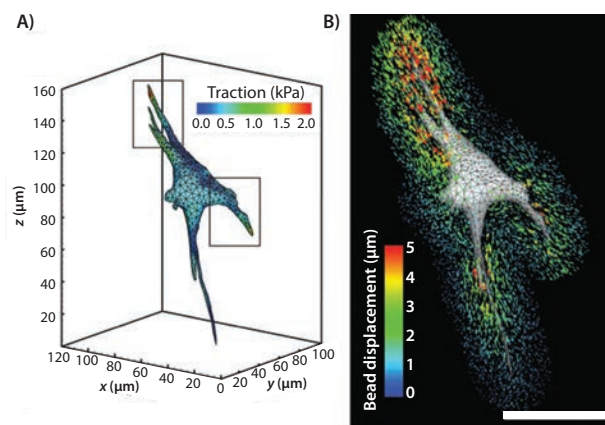


Figure 2. A) A contour plot of the magnitude of the traction forces exerted by a cell in a 3D hydrogel. B) A surface mesh of a cell shown with the bead displacement trajectories. Scale bar represents 50 μm . Adapted from Reference 6 with permission.

Cell Adhesion Force Microscopy (CAFM) is another method used to study cell–matrix interactions. Initially designed to measure the forces required to dislodge inanimate objects from surfaces, it was adapted to study cell–substrate adhesion forces. Developed by Sagvolden et al., this system uses an inclined Atomic Force Microscopy (AFM) cantilever and laser deflection to measure the force required to displace a cell adhered to a substrate.⁸ Combined with an inverted microscope, CAFM can generate force curves associated with dislodging adhered cells.⁸ This system eliminates the necessity of a gel-bead construct while easily integrating with a typical two-dimensional (2D) cell culture setup. However, CAFM is unable to provide the superior spatio-temporal resolution and 3D measurements of TFM.

Not surprisingly, many of the technologies for studying cellular mechanics have been adapted from other fields of study. For example, optical tweezers, originally developed in the field of physics to detect forces on micron-sized particles, have been adapted to study cellular mechanics. Specifically, the effects of the mechanical properties of the extracellular matrix on cell surface proteins can be studied using optical tweezers and microbeads. Choquet et al. first applied optical tweezers to manipulate ligand-coated latex microbeads to study their interaction with murine fibroblasts.⁹ This setup allowed tracking of individual microbead movement in response to cell force and the precise measurement of the forces required to detach beads from adhered cells.⁹ Wang et al. also used microbeads with magnetic twisting cytometry to study cell–ligand interaction. Ligand-coated ferromagnetic microbeads were used to study the effects of varying mechanical loads on specific integrins.¹⁰ In this system, instead of optical tweezers, a strong magnetic field was applied to the ferromagnetic microbeads. A second weaker magnetic field was added orthogonally to twist the microbeads.¹⁰ In this way, mechanical loading on a population of cells can be achieved at a higher throughput as compared to optical tweezers. As such, this system has the potential to study multicellular interactions.

In addition to microbead manipulation, micropads also allow insight into the interaction between a cell and its environment. Galbraith et al. built a force-measuring device consisting of laminin-coated micron-scale pads attached to cantilevers (**Figure 3**). Displacement of these pads in response to fibroblast-generated force was measured. Together with the known mechanical properties of the cantilevers, this setup allowed precise quantification of cell-generated force.¹¹

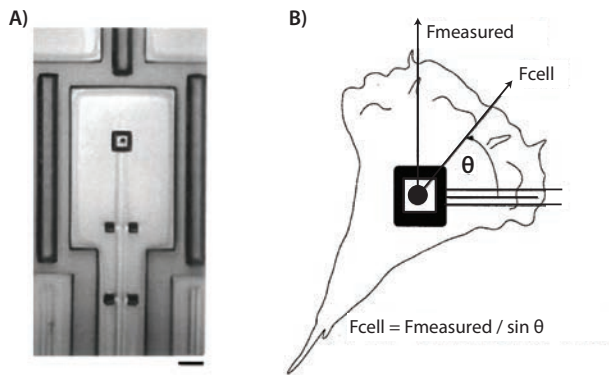


Figure 3. A) A micropad attached to a cantilever in a micromachined device used for studying cellular traction forces. Scale bar represents 10 μm . B) A force diagram illustrating the calculation of traction forces generated by a cell. Adapted from Reference 4 with permission.

The use of microstructures for understanding cellular interactions is not restricted to the study of physical forces. As seen in **Figure 4**, Pinney et al. demonstrated that microrods and microcubes affected the fibrotic response of cardiac cells.¹² By modifying the microenvironment with which the cells interact, a therapeutic response could be achieved without the administration of drugs.¹² Similarly, a nanotubular coating was shown to enhance endothelial healing while decreasing smooth muscle cell proliferation.¹³ These studies into the cellular interactions with micro- and nanostructures give insights to the effects of the physical environment on cellular functions.

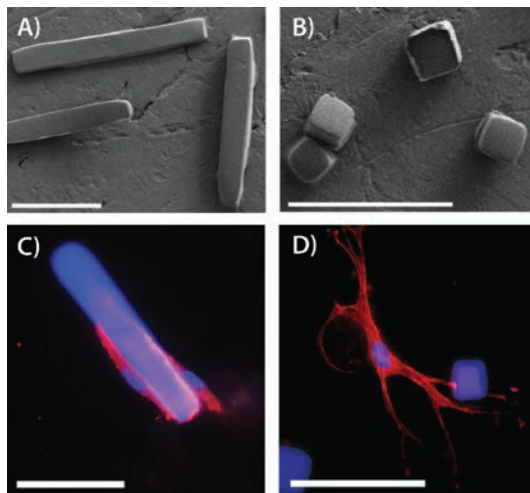


Figure 4. A) Microrods and B) microcubes fabricated from polymerized poly(ethylene glycol) dimethacrylate. Fluorescently stained murine cardiac fibroblasts interacting with microrods (C) and microcubes (D). Scale bar = 50 μm . Adapted from Reference 11 with permission.

The ingenious utilization of advanced materials and technologies has propelled our understanding of cellular interactions. As we continue to develop methodologies at the nanoscale and beyond, the opportunities for answering complex biological questions will continue to grow.

At the Microtissue Level: Characterization

Precise characterization of cellular interactions within a microtissue is necessary to support the advancement of tissue engineering. While biosensors have made substantial advancements in the characterization of biology at the cellular level, their sensitivity and resolution have been creatively applied to study the complexities of multicellular constructs. For example, fluorescent probes also lend themselves well to specific characterization of cell phenotype or biochemical signaling events in

multicellular constructs because they require minimal disruption of the tissue or 3D construct. One example is the study of cell death at the center of multicellular spheroids—an important *in vitro* model used to study multicellular microtissues. Wartenberg et al. used confocal laser scanning microscopy to determine the cell viability in multicellular glioma spheroids.¹⁴ Even though diffusion, light scattering, and absorption of fluorescent dyes present significant limitations and data may be vulnerable to over-interpretation, fluorescent probes remain the best approach to characterizing multicellular construct geometry and viability without perturbing the cells or the structure of the microenvironment.

Inorganic micro- and nanoparticles have also demonstrated a versatility and utility in tissue-level sensing and imaging. Silica nanoparticles with a lipid bilayer coating have been used to great effect in improving fluorescent dye functionality for a variety of biosensing applications.¹⁵ Typically, liposomes rupture in the presence of silica microspheres, fusing around the microsphere and creating a lipid bilayer coating. Using porous silica microspheres, fluorophores can be incorporated into the internal pore space (**Figure 5**). Studies have shown that microspheres with a supported lipid bilayer can protect a pH-sensitive dye, maintaining fluorescence intensity in the presence of a higher pH in the surrounding medium.¹⁵ On the other hand, gold nanoparticles exhibit a higher intensity of absorption and scattering than most organic molecular dyes.¹⁶ These advantages, along with their size-dependent optical and photothermal properties, make gold nanoparticles suitable contrast agents for *in vivo* imaging. Gold nanoparticles, along with gold nanoshells, nanocages, and nanorods, can absorb near-infrared (NIR) light, which can penetrate human tissue to depths of a few centimeters. After absorbing NIR light, gold nanoparticles dissipate heat to the surrounding tissue, thus inspiring applications in imaging, cancer treatment, and tumor ablation.¹⁶

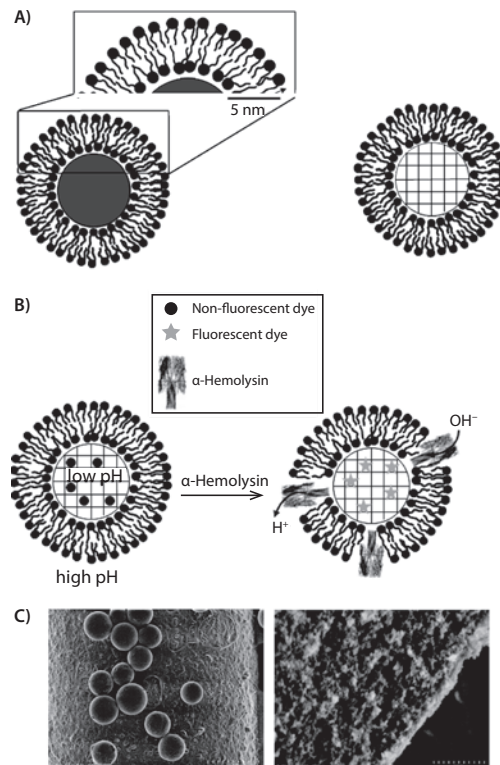


Figure 5. A) Schematic of a solid (left) or porous (right) silica microsphere with a lipid bilayer coating. B) One example of the use of porous silica microspheres. By incorporating alpha hemolysin, a pore is formed within the lipid bilayer, allowing a change in the internal pH and activation of the pH-sensitive dye. C) Scanning electron images of a nonporous microsphere (left) and a porous microsphere (right). High resolution of the porous microsphere details the porous surface. Adapted from Reference 14 with permission.

It is worth highlighting the application of inorganic particles in tissue engineering. Saldanha et al. used iron oxide particles to label and track mesenchymal stem cells (MSCs) using magnetic resonance imaging (MRI) for monitoring articular cartilage regeneration.¹⁷ Labeling MSCs with super-paramagnetic iron oxides prior to transplantation can facilitate longitudinal non-invasive *in vivo* bio-distribution assessment of transplanted cell populations (Figure 6B). The results of this study highlight the need to develop techniques to monitor cell-based tissue engineering strategies for a wide variety of applications.

At the Microtissue Level: Biosensors

Beyond the characterization of microtissues, micro- and nanotechnologies are actively used in the advancement of biosensors. Organic particulates and molecules can be specifically designed to act as biosensors, either as a recognition element for detection of enzymatic or antibody activity, or as a delivery scaffold for other recognition elements. Peptides or proteins conjugated to fluorophores, QDs, or nanoparticles have been used to detect HIV antibodies, bacterial components, and molecules in disease states, such as EGFR in cancer and amyloid plaques in Alzheimer's patients.¹⁸ Polymer-based particulates are commonly developed into spheres and capsules for biosensor applications. One common polymer, poly(lactic-co-glycolic acid) (PLGA), is formed into nanoparticles via a double emulsion method, allowing for the incorporation of hydrophilic or hydrophobic cargo. Nehilla et al. created QD and drug-loaded PLGA nanoparticles for enhanced imaging and drug release applications (Figure 6A).¹⁹

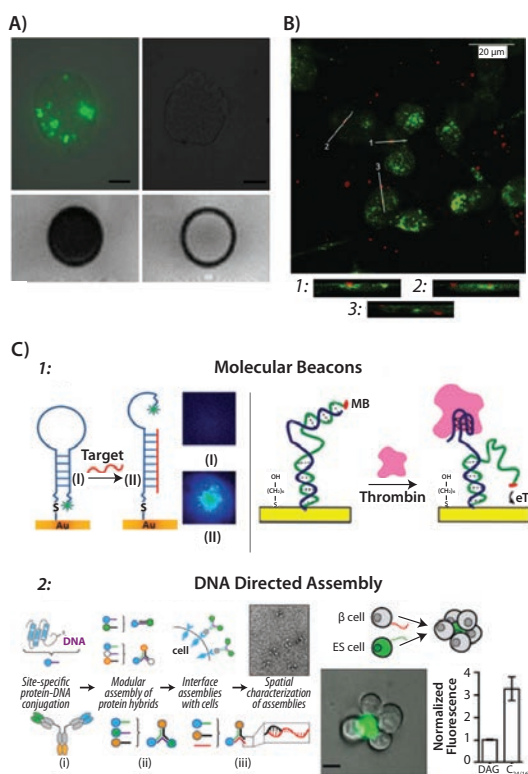


Figure 6. A) Uptake of fluorescently labeled micron-sized iron oxide particles in an MSC line. Left panel: Internalization of labeled particles into the MSC cytoplasm (top left) and successful MRI (2D gradient echo) contrast imaging (bottom left) of the same cells. Right panel: Unlabeled MSCs show no fluorescence (top right) or contrast imaging (bottom right). Scale bar = 10 µm. Adapted from Reference 16 with permission. B) QD-loaded PLGA nanoparticles added to a neuronal cell line (PC12) tissue culture. PC12 cells are labeled with CellTracker Green, while nanoparticles are shown in red. Adapted from Reference 18 with permission. C) Schematic examples of ssDNA biosensor applications. C1: Molecular beacons engineered to detect DNA (left), or the enzyme thrombin (right). C2: DNA-directed assembly of novel protein subunits (left) or novel multicellular aggregates (right). Adapted from References 20,21,23 with permission.

Aside from their applications as a nanoparticulate-based carrier, polymers themselves can be designed to act as biosensors. Common stimulus-responsive polymers include pNIPAM,²⁰ pHEMA,²¹ and pVA-pAA.²² These polymers can be incorporated into hydrogels, polymer brushes, and molecularly imprinted polymer coatings to detect changes in analytes at either the cellular (DNA, FRET, antibody fragments) or multicellular (pH, glucose, and oxygen) levels.²³ Oligonucleotides can also serve as platforms for biosensors. Typically, single-stranded DNA (ssDNA) is immobilized onto a surface such as glass, polymer, or gold nanoparticle via physisorption, chemical crosslinking, or covalent attachment. The phosphate groups of DNA can be used to detect positively charged analytes or dye molecules (Figure 6C).²⁴ Furthermore, DNA strands can form secondary structures that act as molecular beacons to detect DNA, small molecules, and proteins for antibody detection and signal amplification (Figure 6C, left panel).²⁴ Finally, ssDNA and its complimentary counterparts can be utilized toward DNA-directed assembly of novel antibodies²⁵ and multicellular tissues²⁶ which, in turn, can be used for further investigations in both biosensing and tissue characterization²⁷ (Figure 6C, right panel).

Conclusion

It is clear for biologists and engineers that micro- and nanotechnologies are useful tools for studying cells and tissues *in vitro*. However, as it is becoming widely appreciated that the physico-chemical properties of the biomaterial used to study biological systems may affect the structure and functional performance of the system itself, it is important to understand the limitations and caveats of using such materials. For instance, at the multicellular level, the platform used to accommodate and monitor a tissue *in vitro* may trigger phenomena such as tissue inversion and compromise biological performance.²⁸ The mechanisms behind how and why these phenomena happen are yet to be fully understood, but one thing is certain: if we continue the interdependent advancement of materials science and biology, there will be plenty of enlightening answers and engaging questions to follow.

References

- (1) Sawano, A.; Miyawaki, A. *Nucleic Acids Res.* **2000**, *28*, E78.
- (2) Yu, F.; Li, P.; Li, G.; Zhao, G.; Chu, T.; Han, K. *J. Am. Chem. Soc.* **2011**, *133*, 11030–11033.
- (3) Rao, C. N. R.; Ramakrishna Matte, H. S. S.; Voggu, R.; Govindaraj, A. *Dalt. Trans.* **2012**, *41*, 5089.
- (4) Simovic, S.; Song, Y.; Nann, T.; Desai, T. A. *Nanomedicine Nanotechnology, Biol. Med.* **2015**, *11*, 1169–1178.
- (5) Barroso, M. M. *J. Histochem. Cytochem.* **2011**, *59*, 237–251.
- (6) Harris, A. K.; Wild, P.; Stopak, D. *Science.* **1980**, *208* (4440), 177–179.
- (7) Legant, W. R.; Miller, J. S.; Blakely, B. L.; Cohen, D. M.; Genin, G. M.; Chen, C. S. *Nat. Methods* **2010**, *7*, 969–971.
- (8) Sagvolden, G.; Gjaever, I.; Pettersen, E. O.; Feder, J. *Proc. Natl. Acad. Sci. U.S.A.* **1999**, *96*, 471–476.
- (9) Choquet, D.; Felsenfeld, D. P.; Sheetz, M. P. *Cell* **1997**, *88*, 39–48.
- (10) Wang, N.; Butler, J. P.; Ingber, D. E. *Science* **1993**, *260*, 1124–1127.
- (11) Galbraith, C. G.; Sheetz, M. P. *Proc. Natl. Acad. Sci. U.S.A.* **1997**, *94*, 9114–9118.
- (12) Pinney, J. R.; Du, K. T.; Ayala, P.; Fang, Q.; Sievers, R. E.; Chew, P.; Delrosario, L.; Lee, R. J.; Desai, T. A. *Biomaterials* **2014**, *35*, 8820–8828.
- (13) Lee, P. P.; Cerchiari, A.; Desai, T. A. *Nano Lett.* **2014**, 140815113008009.
- (14) Wartenberg, M.; Acker, H. *Micron* **1995**, *26*, 395–404.
- (15) Chemburu, S.; Fenton, K.; Lopez, G. P.; Zeineldin, R. *Molecules* **2010**, *15*, 1932–1957.
- (16) Huang, H.; Barua, S.; Sharma, G.; Dey, S. K.; Rege, K. J. *Controlled Release* **2011**, *155*, 344–357.
- (17) Saldanha, K. J.; Doan, R. P.; Ainslie, K. M.; Desai, T. A.; Majumdar, S. *Magn. Reson. Imaging* **2011**, *29*, 40–49.
- (18) Liu, Q.; Wang, J.; Boyd, B. J. *Talanta* **2015**, *136*, 114–127.
- (19) Nehilla, B. J.; Allen, P. G.; Desai, T. A. *ACS Nano* **2008**, *2*, 538–544.
- (20) Shakhsher, Z.; Seitz, W. R.; Legg, K. D. *Anal. Chem.* **1994**, *66*, 1731–1735.
- (21) Tokarev, I.; Orlov, M.; Katz, E.; Minko, S. J. *Phys. Chem. B* **2007**, *111*, 12141–12145.
- (22) Millington, R. B.; Mayes, A. G.; Blyth, J.; Lowe, C. R. *Anal. Chem.* **1995**, *67*, 4229–4233.
- (23) Lendlein, A.; Shastri, V. P. *Adv. Mater.* **2010**, *22*, 3344–3347.
- (24) Tjong, V.; Tang, L.; Zauscher, S.; Chilkoti, A. *Chem. Soc. Rev.* **2014**, *43*, 1612–1626.
- (25) Liang, S. I.; McFarland, J. M.; Rabuka, D.; Gartner, Z. J. *J. Am. Chem. Soc.* **2014**, *136*, 10850–10853.
- (26) Liu, J. S.; Gartner, Z. J. *Trends Cell Biol.* **2012**, *22*, 683–691.
- (27) Weber, R. J.; Liang, S. I.; Selden, N. S.; Desai, T. A.; Gartner, Z. J. *Biomacromolecules* **2014**, *15*, 4621–4626.
- (28) Cerchiari, A. E.; Garbe, J. C.; Jee, N. Y.; Todhunter, M. E.; Broaders, K. E.; Peehl, D. M.; Desai, T. A.; LaBarge, M. A.; Thomson, M.; Gartner, Z. J. *Proc. Natl. Acad. Sci. U.S.A.* **2015**, *112*, 2287–2292.

Functionalized Gold Nanoparticles

For more information on these products, visit aldrich.com/functionalnano.

Surface	Diameter	Prod. No.
amine functionalized, PEG 3000 coated	5 nm	765260-1ML
	10 nm	765295-1ML
	15 nm	765317-1ML
	20 nm	765333-1ML
	30 nm	765368-1ML
	40 nm	765384-1ML
amine functionalized, PEG 5000 coated	10 nm	765309-1ML
	15 nm	765325-1ML
	20 nm	765341-1ML
	30 nm	765376-1ML
	40 nm	765392-1ML
carboxylic acid functionalized, PEG 3000 coated	5 nm	765430-1ML
	10 nm	765457-1ML
	20 nm	765503-1ML
	40 nm	765554-1ML
	50 nm	765570-1ML
carboxylic acid functionalized, PEG 5000 coated	5 nm	765449-1ML
	10 nm	765465-1ML
	30 nm	765546-1ML
	40 nm	765562-1ML
	50 nm	765589-1ML
methyl terminated, PEG 2000 coated	5 nm	765597-1ML
	10 nm	765619-1ML
	15 nm	765694-1ML
	20 nm	765716-1ML
	30 nm	765635-1ML
	40 nm	765651-1ML
	50 nm	765678-1ML
	50 nm	765686-1ML
methyl terminated, PEG 5000 coated	5 nm	765600-1ML
	10 nm	765627-1ML
	15 nm	765708-1ML
	20 nm	765724-1ML
	30 nm	765732-1ML
	40 nm	765643-1ML
	50 nm	765686-1ML

Gold Nano-Urchins

For more information on these products, visit aldrich.com/goldnanomaterials.

Particle Size, APS (nm)	Absorption, λ_{\max} (nm)	Concentration (mg/mL)	Prod. No.
50	585	4.45E-02	795380-25ML
60	585	4.30E-02	795399-25ML
70	600	~ 4.17E-2	797731-25ML
80	620	~ 4.06E-2	797723-25ML
90	630	3.97E-02	797707-25ML
100	680	~ 3.89E-2	797758-25ML

Silver Nanoparticles

For more information on these products, visit aldrich.com/silvernanomaterials.

Functional Group	Concentration	Average Particle Size (nm)	Prod. No.
PVP	0.02 mg/mL in water	10	795925-25ML
citrate	0.02 mg/mL in 2 mM aqueous sodium citrate	30	796123-25ML
lipoic acid	0.02 mg/mL in water	20	796182-25ML
PEG	0.02 mg/mL in water	40	796301-25ML
BPEI	0.02 mg/mL in water	80	796433-25ML
PVP	0.02 mg/mL in water	100	796018-25ML

Iron Oxide

For more information on these products, visit aldrich.com/functionalnano.

Functional Group	Concentration	Form	Dimension	Prod. No.
amine	Fe 1 mg/mL	dispersion in H ₂ O	diameter 5 nm particle size 4 - 6 nm (TEM)	747343-10ML
	Fe 1 mg/mL	dispersion in H ₂ O	diameter 10 nm particle size 9 - 11 nm (TEM)	747300-10ML
	Fe 1 mg/mL	dispersion in H ₂ O	diameter 30 nm particle size 28 - 32 nm (TEM)	747327-10ML
biotin	Fe 1 mg/mL	dispersion in H ₂ O	diameter 5 nm particle size 4 - 6 nm (TEM)	747416-1ML
	Fe 1 mg/mL	dispersion in H ₂ O	diameter 10 nm particle size 9 - 11 nm (TEM)	747424-1ML
	Fe 1 mg/mL	dispersion in H ₂ O	diameter 30 nm particle size 28 - 32 nm (TEM)	747432-1ML
carboxylic acid	Fe 5 mg/mL	dispersion in H ₂ O	diameter 10 nm particle size 9 - 11 nm (TEM)	747254-2ML
	Fe 5 mg/mL	dispersion in H ₂ O	diameter 30 nm particle size 28 - 32 nm (TEM)	747335-2ML
PEG	Fe 1 mg/mL	dispersion in H ₂ O	diameter 5 nm particle size 4 - 6 nm (TEM)	790508-10ML
	Fe 1 mg/mL	dispersion in H ₂ O	diameter 10 nm particle size 9 - 11 nm (TEM)	747319-10ML
	Fe 1 mg/mL	dispersion in H ₂ O	diameter 30 nm particle size 28 - 32 nm (TEM)	747408-10ML
N-succinimidyl ester	-	powder	diameter 5 nm particle size 4 - 6 nm (TEM)	747440-1G
	-	powder	diameter 10 nm particle size 9 - 11 nm (TEM)	747459-1G
	-	powder	diameter 30 nm particle size 28 - 32 nm (TEM)	747467-1G

Fluorescent Nanodiamonds

For more information on these products, visit aldrich.com/nanodiamonds.

Particle Size (nm)	Description	Concentration	Prod. No.
70	>300NV/particle	1 mg/mL in deionized water	798169-5ML
90	>500NV/particle	1 mg/mL in deionized water	798150-5ML
100	>400NV/particle	1 mg/mL in deionized water	798142-5ML
100	>800NV/particle	1 mg/mL in deionized water	798134-5ML
120	>1200NV/particle	1 mg/mL in deionized water	798088-5ML

Fluorescent Silica Nanobeads

For more information on these products, visit aldrich.com/ceramicnano.

Name	Emission Max (nm)	Absorption Max (nm)	Particle Size (nm)	Prod. No.
Fluorescent silica nanobeads	570	~ 590	25	797928-5MG
	570	~ 590	50	797936-5MG
	590	~ 555	90	797898-5MG
	590	555	120	797863-5MG
Ultrastable fluorescent silica nanobeads	590	555	25	797901-2MG
	590	~ 555	50	797952-2MG
	590	~ 555	90	797944-2MG
	590	~ 555	120	797871-2MG

Preformed PLGA Biodegradable Particles

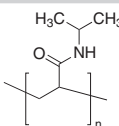
For more information on these products, visit aldrich.com/biopoly.

Name	Average Diameter	Prod. No.
PLGA nanoparticles	100 nm	805092-50MG
	200 nm	805106-50MG
	500 nm	805149-50MG
PLGA microspheres	2 μ m	805130-50MG
	25 μ m	805114-50MG
	50 μ m	805122-50MG
Green fluorescent PLGA nanoparticles	100 nm	805157-50MG
	200 nm	805211-50MG
	500 nm	805300-50MG
Green fluorescent PLGA microspheres	2 μ m	805181-50MG
	25 μ m	805173-50MG
	50 μ m	805165-50MG

Biosensor Polymers (Stimulus-responsive Polymers)

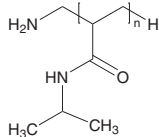
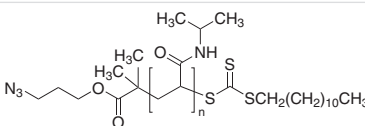
Poly(*N*-isopropylacrylamide) (PNIPAM)

For more information on these products, visit aldrich.com/polynipam.

Name	Structure	Molecular Weight	Prod. No.
Poly(<i>N</i> -isopropylacrylamide)		M_n 20,000-40,000	535311-10G

End-functionalized PNIPAM

For more information on these products, visit aldrich.com/polynipam.

Name	Structure	Molecular Weight	Prod. No.
Poly(<i>N</i> -isopropyl acrylamide), amine terminated		average M_n 2,000	799564-1G
		average M_n 5,000	802107-1G
Poly(<i>N</i> -isopropylacrylamide), azide terminated		average M_n 15,000	747068-1G 747068-5G

End-functionalized PNIPAM (*cont'd*)

Name	Structure	Molecular Weight	Prod. No.
Poly(<i>N</i> -isopropylacrylamide), carboxylic acid terminated		average M_n 2,000	724815-1G 724815-5G
		average M_n 5,000	724807-1G 724807-5G
		average M_n 7,000	724866-1G 724866-5G
		average M_n 10,000	724459-5G
		average M_n 2,000	731048-1G 731048-5G
Poly(<i>N</i> -isopropylacrylamide), maleimide terminated		average M_n 2,000	728632-1G 728632-5G
		average M_n 5,500	

PolyNIPAM Copolymers

For more information on these products, visit aldrich.com/polynipam.

Name	Structure	Molecular Weight/Viscosity	Prod. No.
Poly(<i>N</i> -isopropylacrylamide- <i>co</i> -acrylic acid)		viscosity 7500-12500 5% in H ₂ O	741930-5G
Poly(<i>N</i> -isopropylacrylamide- <i>co</i> -acrylamide)		average M_n 20,000	738727-5G
Poly(<i>N</i> -isopropylacrylamide- <i>co</i> -butylacrylate)		average M_n 30,000	762857-5G
Poly(<i>N</i> -isopropylacrylamide- <i>co</i> -methacrylic acid)		average M_n 8,000-10,000	750166-5G
		average M_n 50,000	724467-5G

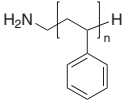
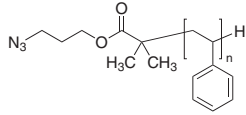
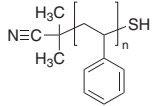
Polymethacrylates

For more information on these products, visit aldrich.com/polymethacrylates.

Name	Structure	Molecular Weight	Prod. No.
Poly(2-hydroxyethyl methacrylate)		average M_v 20,000	529265-5G 529265-25G
		average M_v 300,000	192066-10G 192066-25G
		average M_v 1,000,000	529257-1G 529257-10G
Poly(hydroxyethyl methacrylate), DDMAT terminated		average M_n 7,000	772542-1G

Functional Polystyrene for Particle Formation and Conjugation

For more information on these products, visit aldrich.com/polystyrenes.

Name	Structure	Molecular Weight	PDI	Prod. No.
Polystyrene, amine terminated		average M_n 5,000	≤ 1.2	791164-1G
		average M_n 10,000	≤ 1.3	791067-1G
Polystyrene, azide terminated		average M_n 5,000	≤ 1.3	791156-1G
		average M_n 15,000	≤ 1.3	746916-1G
Polystyrene, thiol terminated		average M_n 5,000	≤ 1.1	746924-1G
		average M_n 11,000	≤ 1.1	746932-1G



ALDRICH
Materials Science

MATERIALS FOR INNOVATION

BIOMEDICAL

Materials for drug delivery, tissue engineering, and regenerative medicine; PEGs, biodegradable and natural polymers; functionalized nanoparticles; block copolymers, dendrimers and nanoclays

ELECTRONICS

Nanowires; printed electronics inks and pastes; materials for OPV, OFET, OLED; nanodispersions; CNTs and graphene; precursors for PVD, CVD, and sputtering

ENERGY

Ready-to-use battery grade electrode and electrolyte materials; nanopowders, nanostructures and dispersions; quantum dots; perovskites; fuel cells and membrane; hydrogen storage materials including MOFs; phosphors; thermoelectrics; high purity salts

Find more information on our capabilities at

aldrich.com/matsci

INJECTABLE HYDROGELS

FOR CELL DELIVERY AND TISSUE REGENERATION



Prathamesh M. Kharkar,¹ April M. Kloxin^{1,2*}
¹Materials Science and Engineering and ²Chemical and Biomolecular Engineering
 University of Delaware, Newark, DE 19716 USA
 *Email: akloxin@udel.edu

Introduction

The use of hydrogel-based biomaterials for the delivery and recruitment of cells to promote tissue regeneration in the body is of growing interest.¹ Hydrogels are hydrophilic, water-swollen polymer networks formed from a variety of natural and synthetic polymeric building blocks (**Figure 1**). These building blocks have been engineered to enable crosslinking by chemical reaction or through physical interactions in the presence of cells and proteins that proceeds rapidly enough for injection and *in situ* hydrogel formation. In this article, we review principles for the design of these injectable hydrogels, advances in polymers and chemistries for their formation, and recent examples of their application for tissue regeneration.

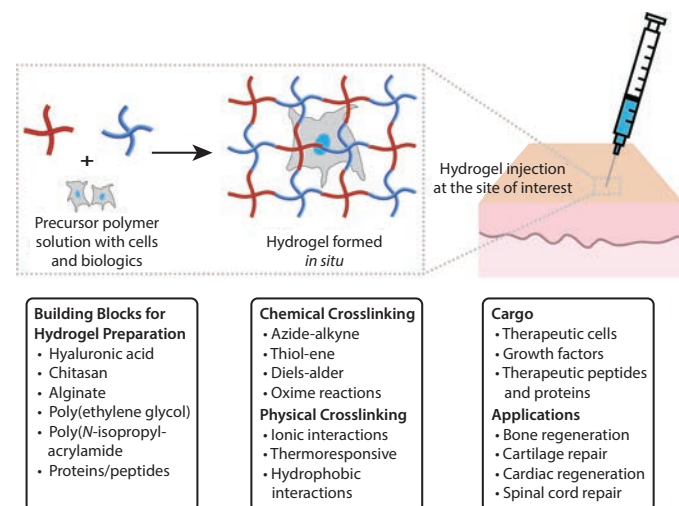


Figure 1. Injectable hydrogels for cell delivery and tissue engineering applications. Injectable hydrogels can be prepared using a variety of natural and synthetic polymers, recombinant proteins, and peptides. These base materials have been crosslinked in the presence of cells, biologics, and tissues using chemical reactions or physical interactions. Such injectable hydrogels formed *in situ* have been used to deliver various therapeutic cells or biologics (e.g., growth factors, chemokines for modulating the function endogenous cells) to promote the regeneration of tissues, including bone, cartilage, and skin (depicted here).

Polymeric Building Blocks for the Design of Injectable Hydrogels

Injectable hydrogels are prepared using a wide range of materials. Cyto- and bio-compatibility as well as reactive chemistries are critical factors for selecting base materials that can be used in hydrogels for cell delivery or recruitment in the body. Material crosslinking (formation and concentration of physical or covalent linkages), biodegradability, and biochemical properties are also important design criteria that can influence the structural, mechanical, and biological properties of the hydrogels initially and over time. In addition, the base polymeric materials must be stable in either solid or solution form for storage prior to use in translational or clinic studies.

The hydrophilic polymers used for hydrogel construction generally can be divided into two categories: natural polymers derived from tissues or other natural sources and synthetic polymers fabricated using organic chemistry and molecular engineering principles. Biocompatible natural polymers such as hyaluronic acid, chitosan (**Aldrich Prod. Nos. 448869, 448877, and 419419**), heparin, alginate, fibrin (**Sigma Prod. No. F5386**), collagen (**Aldrich Prod. Nos. 804592, 804622, and 804614**), chondroitin sulfate, and silk, mimic aspects of the native microenvironment, including its mechanical and biochemical properties for modulating cell adhesion, migration, and other key functions for tissue regeneration.² These natural polymers have been used as building blocks for injectable hydrogel formation by physical (e.g., ionic, hydrogen bonding) or covalent crosslinking (e.g., reaction of functional groups on modified polymers).³ Synthetic polymers such as poly(ethylene glycol) [PEG], poly(vinyl alcohol) [PVA], poly(*N*-isopropylacrylamide) [PNIPAAm], and polycaprolactone [PCL] have frequently been used for the design of injectable, cell-compatible hydrogels due to their commercial availability, low batch-to-batch variation, versatility for chemical modification, and consequently, the ease of tuning the mechanical properties of the resulting hydrogels. Since synthetic polymers lack the inherent biochemical cues for interaction with cells, they are used in combination with natural polymers or biomimetic peptides to facilitate cell adhesion, migration, and protein secretion.

To capture the favorable attributes of both traditional natural and synthetic polymers, synthetic peptides and recombinant proteins have been designed for injection and subsequent assembly *in situ* for cell delivery. Examples of such combinations include resilin-containing proteins, tryptophan- and proline-rich sequences in mixing-induced two-component hydrogels (MITCH), and peptide amphiphiles with hydrophilic peptide segments (lysine or glutamic acid repeats) conjugated to a hydrophobic fatty acid.⁴ These designer building blocks have been engineered with integrin-binding peptide sequences to promote cell adhesion and degradable sequences for cell-driven remodeling. Here, we will focus on several polymers commonly used in designing injectable hydrogels for cell delivery and tissue regeneration.

Hyaluronic acid (HA) (**Sigma Prod. No. H5542**) is a non-immunogenic, biocompatible glycosaminoglycan found in the extracellular matrix of connective, epithelial, and neural tissues. HA-based biomaterials degrade *in vivo* in response to hyaluronidase and have been used for various biomedical applications.⁵ Young et al. reported use of injectable HA hydrogels for the delivery of retinal progenitor cells (RPC) for retinal repair.⁶ Commercially available thiol-functionalized HA was reacted with acrylate-functionalized PEG to form chemically crosslinked hydrogels in the presence of mouse retinal progenitor cells. Injected hydrogels resulted in even distribution of RPCs within subretinal space that differentiated toward desired photoreceptors. HA has been modified with a number of reactive functional groups relevant for *in situ* formation upon injection.⁷ In a recent example, Burdick et al. modified HA with aldehyde and hydrazine functional groups to create injectable hydrogels that released a recombinant tissue inhibitor of matrix metalloproteinases (TIMP3) and modulates the activities of myofibroblasts for the improved regeneration of tissue after myocardial infarction.⁸

Alginate, (**Aldrich Prod. No. 180947**), a cationic biopolymer obtained from brown algae, previously has been used in several clinical applications, including as a wound dressing material. In the presence of divalent cations, alginate forms physically crosslinked hydrogels in which the mechanical properties can be tuned by varying the polymer amount, molecular weight, and the concentration of crosslinkable cations. Alginate-based injectable hydrogels have been used for the regeneration of a variety of tissues, including bone, cartilage, adipose, and cardiac tissues.⁹ Kim et al. demonstrated adipose tissue formation by injecting alginate hydrogels loaded with preconditioned cryopreserved human adipose stem cells (hADSCs) *in vivo* in mice.¹⁰ Prior to injection, alginate was oxidized to improve its biodegradability and modified using carbodiimide chemistry with an integrin-binding peptide (G₁RGDASSKY) to promote cell adhesion. In 10 weeks, hydrogels containing hADSCs resulted in the formation of adipose tissue (~50% of initial gel volume), where a negative control (hydrogels without cells) lacked new tissue formation. In addition to HA and alginate, injectable hydrogels have been prepared using a variety of other natural polymers, including chitosan, heparin, collagen, gelatin, chondroitin sulfate, or combinations of these, for cartilage, bone, and cardiac tissue regeneration.¹¹

PEG is one of the most widely used synthetic polymers for the preparation of injectable hydrogels due to its biocompatibility and lack of protein binding sites. PEG provides a relatively bioinert base for the introduction of specific bioactive groups (e.g., peptides) to modulate interactions with cells and has been modified with a variety of end groups, including amines, thiols, maleimides, acrylates, and norbornenes, that are easily synthesized or obtained commercially.¹² Several research groups including ours have developed PEG-based hydrogels for cell delivery and tissue regeneration. For example, Garcia et al. recently used PEG macromers functionalized with maleimides and peptides functionalized with thiols (i.e., cysteines) to form injectable hydrogels for cell delivery.¹³ These hydrogels maintained the viability of progenitor cells (C2C12s) (**Sigma Prod. No. 91031101**) during encapsulation, where crosslinking times ranged between 1–5 minutes based on the polymer concentration, and promoted cell spreading.

Crosslinking and Degradation Reactions for Controlling Hydrogel Formation and Erosion

Injectable hydrogels are formed using a variety of chemical or physical crosslinking strategies which must be carefully selected to match the specific application of interest. For example, an appropriate crosslinking rate is essential for the proper formation of an injectable hydrogel *in situ*. If the gelation is too slow, precursors are likely to perfuse from the site of injection into surrounding tissues, leading to poor hydrogel properties and potentially to an inflammatory response to unreacted monomers. If the gelation is too rapid, shear thinning (and potentially premature gel formation) in the syringe may occur, introducing network defects that, in turn, affect gel mechanical properties and retention/release of cargo (i.e., cells). In addition, the ability to form the hydrogel in the presence of live cells and therapeutic proteins is the key for cell delivery and regenerative medicine applications. The following discussion will highlight a few relevant crosslinking techniques with recent examples.

Due to its rapid crosslinking kinetics and high efficiency, click chemistry represents one of the most attractive classes of crosslinking chemistries for the formation of hydrogels for cell delivery. Commonly used copper catalyzed alkyne-azide click reactions have been utilized to form hydrogels;¹⁴ however, copper can be cytotoxic and its use limits applicability in cell encapsulation and delivery applications. To overcome this, strain promoted azide-alkyne cycloadditions (SPAAC) have been utilized to crosslink cytocompatible hydrogels. DeForest and Anseth reported the use of SPAAC for fibroblast encapsulation in hydrogels.¹⁵ The authors showed that when a four-arm PEG end-functionalized with difluorinated cyclooctyne is reacted with an azide-functionalized peptide crosslinker, the ring strain and electron-withdrawing fluorine substituents promote a rapid crosslinking reaction (~2 minutes) without a catalyst. In another approach, Dove et al. recently reported the catalyst-free reaction of azide-functionalized chitosan with propionic acid-functionalized PEG to form hydrogels in the presence of cells.¹⁶ The authors were able to encapsulate mesenchymal stem cells during hydrogel formation and showed the encapsulated cells exhibit high viability after 24 hours of culture (>95%). These and other click reactions, including thiol-enes (in particular, Michael additions of thiols with maleimides or vinyl sulfones), Diels-Alder, aldehyde-hydrazine, and oxime reactions, are attractive for injectable hydrogel applications. For a comprehensive summary of chemical crosslinking reactions, readers are referred to recent review articles.^{3,12,17}

Physically crosslinked injectable hydrogels have been formed using ionic, hydrophobic, hydrogen bonding, or guest-host interactions, most commonly through thermoresponsive and ionic interactions.¹⁸ Reis et al. reported formation of injectable hydrogels using thermoresponsive poly(*N*-isopropylacrylamide)-*g*-methylcellulose (PNIPAAm-*g*-MC) for cartilage tissue engineering applications.¹⁹ Hydrogel formation was achieved using the thermoresponsive phase transition of the PNIPAAm-*g*-MC polymer with gelation occurring above its lower critical solution temperature (~32 °C). Encapsulated ATDC5 chondrogenic cells adopted a rounded morphology, supporting maintenance of the chondrocyte phenotype, which is critical for articular cartilage regeneration. Physical crosslinking using ionic interactions is extensively used to crosslink polysaccharides such as alginate and chitosan. For example, Xu et al. encapsulated human umbilical cord mesenchymal stem cells (hUCMSCs) in alginate-based injectable hydrogels for bone tissue engineering.²⁰ Gelation of alginate was achieved by crosslinking with calcium, a divalent cation in the presence of hUCMSCs with a viability of ~70% post-encapsulation.

For all cell delivery and tissue regeneration applications, hydrogels must degrade in a controlled manner after injection for the desired therapeutic use (e.g., cell release or infiltration, protein elaboration) without cytotoxic degradation byproducts. Typically, degradation can be achieved using cleavable polymeric backbones or dynamic/reversible crosslinks. As mentioned earlier, natural polymers such as hyaluronic acid and alginate undergo enzymatic hydrolysis *in vivo*, providing a mechanism for hydrogel degradation. For synthetic polymers, hydrogels have been traditionally engineered with ester linkages like poly(lactic acid) for degradation by ester hydrolysis in aqueous microenvironments preprogrammed based on the number of esters incorporated. In addition, several research groups have explored additional responsive or triggerable degradable chemistries, including photodegradation,²¹ retro Michael type,²² and retro Diels-Alder reactions,²³ for precise control over material degradation *in situ*. More recently, in collaboration with the Kiick research group, we have achieved precise control over the degradation of injectable hydrogels formed with thiol-maldehyde chemistry by incorporating two or more modes of degradation using combinations of these chemistries.²⁴ Hydrogel degradation over multiple time scales was achieved by incorporation of: i) *o*-nitrobenzyl ether linkages that undergo photodegradation ($k \sim 10^{-1} \text{ min}^{-1}$ for 365 nm to 10^{-2} min^{-1} for 400–500 nm); ii) aryl-thiol-based succinimide thioether linkages that undergo retro Michael-type reaction in the presence of glutathione ($k \sim 10^{-3} \text{ min}^{-1}$); and iii) ester linkages that undergo ester hydrolysis in aqueous microenvironments ($k \sim 10^{-4} \text{ min}^{-1}$). In principle, such injectable hydrogels with multimodal degradability could be utilized to deliver or recruit cells with precise and tailorable control over gel degradation and release profiles for tissue regeneration.

Cell Delivery and Tissue Regeneration with *in situ* Forming Hydrogels

Injectable hydrogels have been used to deliver a variety of cargo molecules, including growth factors, chemokines, and therapeutic cells to promote tissue regeneration *in vitro* and *in vivo*. These *in situ* forming materials are being used for the regeneration of a variety of tissues,

including bone, cartilage, intervertebral disc, adipose, cardiac, and vascular tissues. A few recent examples of injectable hydrogels used for bone, cartilage, and cardiac tissue regeneration are highlighted here. A comprehensive review of this growing research area can be found in recent a review article.²⁵

Bone

Addressing bone defects and abnormalities is one of the key challenges in orthopedics. Bone tissue engineering strategies using injectable hydrogels provide an attractive alternative to traditional treatments, such as autologous bone implantation and bone graft materials, as demonstrated in seminal works by Hubbell et al.²⁶ Recently, Song et al. investigated the use of injectable thermoresponsive poly(phosphazene)-based hydrogels for sustained delivery of bone morphogenetic protein-2 (BMP-2) (**Sigma Prod. No. H4791**).²⁷ Poly(phosphazene) with additional carboxylic groups, which promote ionic interactions with BMP-2, were used to form hydrogels upon injection, where gelation occurs as the temperature approaches physiological temperature (37 °C). Prolonged release of BMP-2 from such hydrogels over 20 days was achieved *in vitro* and resulted in significantly higher osteocalcin secretion ($\sim 14 \text{ ng/mL}$) by C2C12 cells (**Sigma Prod. No. 91031101**) compared to the control ($\sim 2 \text{ ng/mL}$), suggesting retention of the bioactivity of BMP-2 for osteoblastic differentiation. Injection of the BMP-2 loaded hydrogels *in vivo* resulted in ectopic bone formation in mice, highlighting the promise of injectable hydrogels for bone regeneration.

Cartilage

Due to the limited self-healing capacity of cartilage tissues, a variety of surgical treatments have been developed to promote cartilage regeneration. Among these, use of injectable or *in situ* forming hydrogels to deliver growth factors and therapeutic cells at the site of the cartilage defect is one emerging strategy.²⁸ Jin et al. reported injectable and biodegradable hydrogels formed using dextran and hyaluronic acid for cartilage tissue engineering. Rapid hydrogel formation (~ 2 minutes) was achieved using oxidative coupling of phenolic groups in the presence of horseradish peroxidase (**Sigma Prod. No. 77332**) and hydrogen peroxide (H_2O_2 , **Sigma-Aldrich Prod. No. H3410**). Bovine chondrocytes maintain

HAVE YOU MISSED OUR RECENT ISSUES?

- Vol. 10 No. 3: Alternative Energy Generation and Storage (RRB)
- Vol. 10 No. 2: Graphene and Carbon Materials (ROM)
- Vol. 10 No. 1: 10th Anniversary Issue—Materials that Matter (RJO)
- Vol. 9 No. 4: Materials for Energy Harvesting and Storage (REO)
- Vol. 9 No. 3: Polymers in Therapeutics and Nanomedicine (QZP)
- Vol. 9 No. 2: Inorganic Materials in Biomedical Applications (QIV)

To view a complete library of issues or to subscribe to our newsletter, visit

aldrich.com/materialmatters



high cell viability during the encapsulation process (~95%) and exhibit increased glycosaminoglycan and collagen production over 21 days. For these types of repairs, surgery is requisite for accessing the tissue site. Consequently, other reactive chemistries that enable rapid, triggered gel formation *in situ* also have been utilized (e.g., photopolymerized methacrylate or thiol–ene systems²⁹) and represent active areas of research for tissue regeneration in non-uniform defect sites. Such *in situ* forming hydrogels are promising for the repair of cartilage defects.

Cardiovascular Tissues

Cardiovascular disease is another challenging area where injectable hydrogels offer promising treatment options. To address challenges associated with chronic myocardial infarction, Park et al. developed thiol–ene hydrogels that use acrylated hyaluronic acid and a thiol-containing MMP-sensitive peptide crosslinker to modulate cellular activities toward tissue regeneration.³⁰ Specifically, a chemokine, stromal-derived factor-1, (SDF-1) (Sigma Prod. Nos. SRP3253 and SRP3276) that plays a key role in repair of myocardial infarction and Ac-SDKP (a peptide that stimulates endothelial cell proliferation and angiogenesis) were incorporated within the hydrogel precursor solution. Protein-laden hydrogels were formed upon injection into the epicardium in a myocardial infarction model and heart functions were evaluated after 4 weeks. These evaluations showed that injection of SDF-1 and SDKP laden hydrogels improved ventricle function, increased angiogenesis, decreased infarct size (~8% for SDF-1/SDKP compared to ~41% for control), and increased wall thickness (211% higher compared to control) within the infarct region. These results demonstrate the utility of injectable hydrogels for modulating cellular functions, including endogenous cells, for tissue regeneration.

Conclusion

Over the past decade, injectable hydrogels have emerged as promising biomaterials for cell delivery or recruitment for promoting tissue regeneration. Significant advancements have been made in the design of the base polymers and crosslinking chemistries for hydrogel formation and the cleavable and reversible chemistries for hydrogel degradation, both in the presence of cells and tissues. These approaches maintain the bioactivity of delivered therapeutic cells and biologics and are leading to advances in the quality and function of regenerated tissues.

Acknowledgments

The authors gratefully acknowledge support for related work from the Delaware COBRE program with a grant from the National Institute of General Medical Sciences (NIGMS P20GM104316-02), from the National Institutes of Health, the Burroughs Wellcome Fund, and the University of Delaware Research Foundation. We thank the MediaLab in the Department of Biochemistry at the University of Wisconsin at Madison for the use of an Adobe Illustrator template.

References

- (1) (a) Slaughter, B. V.; Khurshid, S. S.; Fisher, O. Z.; Khademhosseini, A.; Peppas, N. A. *Adv Mater* **2009**, *21* (32–33), 3307–3329; (b) Rehmann, M. S.; Kloxin, A. M. *Soft matter* **2013**, *9* (29), 6737–6746.
- (2) Munarin, F.; Petrini, P.; Bozzini, S.; Tanzi, M. C. *J Appl Biomater Funct Mater* **2012**, *10* (2), e67–81.
- (3) Kharkar, P. M.; Kiick, K. L.; Kloxin, A. M. *Chem Soc Rev* **2013**, *42* (17), 7335–72.
- (4) Sun, J. E.; Pochan, D., *Peptidic Hydrogels*. In *In-Situ Gelling Polymers*, Springer: **2015**; pp 127–150.
- (5) Burdick, J. A.; Prestwich, G. D. *Adv Mater* **2011**, *23* (12), H41–56.
- (6) Liu, Y.; Wang, R.; Zarebinski, T. I.; Doty, N.; Jiang, C.; Regatieri, C.; Zhang, X.; Young, M. J. *Tissue Eng Part A* **2013**, *19* (1–2), 135–42.
- (7) Burdick, J. A.; Prestwich, G. D. *Adv Mater* **2011**, *23* (12), H41–H56.
- (8) Purcell, B. P.; Lobb, D.; Charati, M. B.; Dorsey, S. M.; Wade, R. J.; Zellars, K. N.; Doviak, H.; Pettaway, S.; Logdon, C. B.; Shuman, J. A. *Nat Mater* **2014**, *13* (6), 653–661.
- (9) Bidarra, S. J.; Barrias, C. C.; Granja, P. L. *Acta Biomater* **2014**, *10* (4), 1646–62.
- (10) Kim, W. S.; Mooney, D. J.; Arany, P. R.; Lee, K.; Hubsch, N.; Kim, J. *Tissue Eng Part A* **2012**, *18* (7–8), 737–743.
- (11) Munarin, F.; Petrini, P.; Bozzini, S.; Tanzi, M. C. *J Appl Biomater Funct Mater* **2012**, *10* (2), 67–81.
- (12) Bakaic, E.; Smeets, N. M. B.; Hoare, T. *RSC Adv* **2015**, *5* (45), 35469–35486.
- (13) Phelps, E. A.; Enemchukwu, N. O.; Fiore, V. F.; Sy, J. C.; Murthy, N.; Sulchek, T. A.; Barker, T. H.; Garcia, A. J. *Adv Mater* **2012**, *24* (1), 64–70, 2.
- (14) Adzima, B. J.; Tao, Y.; Kloxin, C. J.; DeForest, C. A.; Anseth, K. S.; Bowman, C. N. *Nat Chem* **2011**, *3* (3), 256–59.
- (15) DeForest, C. A.; Anseth, K. S. *Nat Chem* **2011**, *3* (12), 925–931.
- (16) Truong, V. X.; Ablett, M. P.; Gilbert, H. T. J.; Bowen, J.; Richardson, S. M.; Hoyland, J. A.; Dove, A. P. *Biomater Sci* **2014**, *2* (2), 167–175.
- (17) Nimmo, C. M.; Shoichet, M. S. *Bioconjugate Chem* **2011**, *22* (11), 2199–2209.
- (18) Wang, H.; Heilshorn, S. C. *Adv Mater* **2015**, *27* (25), 3717–3736.
- (19) Sá-Lima, H.; Tuzlakoglu, K.; Mano, J. F.; Reis, R. L. *J Biom* **2011**, *98* (4), 596–603.
- (20) Zhao, L.; Weir, M. D.; Xu, H. H. *Biomaterials* **2010**, *31* (25), 6502–6510.
- (21) Kloxin, A. M.; Kasko, A. M.; Salinas, C. N.; Anseth, K. S. *Science* **2009**, *324* (5923), 59–63.
- (22) Baldwin, A. D.; Kiick, K. L. *Polym Chem* **2013**, *4* (1), 133–143.
- (23) Koehler, K. C.; Anseth, K. S.; Bowman, C. N. *Biomacromolecules* **2013**, *14* (2), 538–547.
- (24) (a) Kharkar, P. M.; Kloxin, A. M.; Kiick, K. L. *J Mat Chem B* **2014**, *2* (34), 5511–5521; (b) Kharkar, P. M.; Kiick, K. L.; Kloxin, A. M. *Polym Chem* **2015**, *6* (31), 5565–5574.
- (25) (a) Bae, K. H.; Wang, L. S.; Kurisawa, M. *J Mat Chem B* **2013**, *1* (40), 5371–5388; (b) Bakaic, E.; Smeets, N. M. B.; Hoare, T. *RSC Advances* **2015**, *5* (45), 35469–35486; (c) Bidarra, S. J.; Barrias, C. C.; Granja, P. L. *Acta Biomaterialia* **2014**, *10* (4), 1646–1662; (d) Huynh, C. T.; Nguyen, M. K.; Lee, D. S. *Macromolecules* **2011**, *44* (17), 6629–6636; (e) Amini, A. A.; Nair, L. S. *Biomedical Materials* **2012**, *7* (2), 024105.
- (26) Lutolf, M.; Lauer-Fields, J.; Schmoekel, H.; Metters, A.; Weber, F.; Fields, G.; Hubbell, J. *Proc Natl Acad Sci USA* **2003**, *100* (9), 5413–5418.
- (27) Seo, B.-B.; Choi, H.; Koh, J.-T.; Song, S.-C. *J Controlled Release* **2015**, *209*, 67–76.
- (28) (a) Johnstone, B.; Alini, M.; Cucchiari, M.; Dodge, G. R.; Eglon, D.; Guilak, F.; Madry, H.; Mata, A.; Mauck, R. L.; Semino, C. E. *Eur Cell Mater* **2013**, *25* (248), e67; (b) Spiller, K. L.; Maher, S. A.; Lowman, A. M. *Tissue Eng Part B* **2011**, *17* (4), 281–299.
- (29) (a) Lin, C. C.; Ki, C. S.; Shih, H. *J Appl Polym Sci* **2015**, *132* (8); (b) Sawicki, L. A.; Kloxin, A. M. *Biomater Sci* **2014**, *2* (11), 1612–1626.
- (30) Song, M.; Jang, H.; Lee, J.; Kim, J. H.; Kim, S. H.; Sun, K.; Park, Y. *Biomaterials* **2014**, *35* (8), 2436–2445.

Poly(ethylene glycol) and Poly(ethylene oxide)

Multi-arm PEGs

For more information on these products, visit aldrich.com/peg.

Name	Molecular Weight	Prod. No.
4-arm Poly(ethylene glycol) norbornene terminated	average M_n 10,000	808474-1G
	average M_n 20,000	808466-1G
Poly(ethylene oxide), 4-arm, amine terminated	average M_n 10,000	565733-250MG 565733-1G
Poly(ethylene oxide), 4-arm, carboxylic acid terminated	average M_n 10,000	565717-500MG 565717-1G
Poly(ethylene oxide), 4-arm, hydroxy terminated	average M_n 10,000	565709-1G 565709-5G
Poly(ethylene oxide), 6-arm, hydroxy terminated	average M_n 17,000	570273-250MG 570273-1G
Poly(ethylene oxide), 4-arm, succinimidyl glutarate terminated	average M_n 10,000	565768-250MG 565768-1G
Poly(ethylene oxide), 4-arm, succinimidyl succinate terminated	average M_n 10,000	565741-250MG 565741-1G
Poly(ethylene oxide), 4-arm, thiol terminated	average M_n 10,000	565725-1G

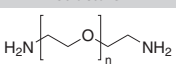
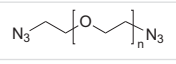
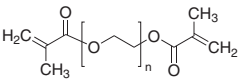
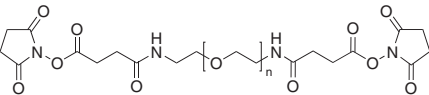
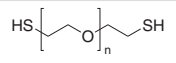
Multi-arm Block Copolymers

For more information on these products, visit aldrich.com/peg.

Name	Molecular Weight	PDI	Prod. No.
Poly(ethylene oxide)- <i>block</i> -polylactide, 4-arm	poly(ethylene oxide) M_n 2,500 polylactide average M_n 3,500	< 1.2	570354-250MG 570354-1G
Poly(ethylene oxide)- <i>block</i> -polycaprolactone, 4-arm	PCL average M_n 2,500 PEG average M_n 2,500 average M_n 5,000 (total)	< 1.2	570346-1G

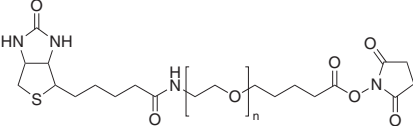
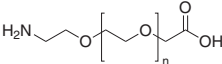
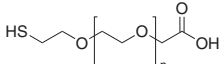
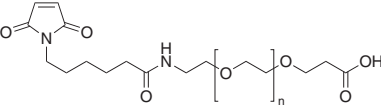
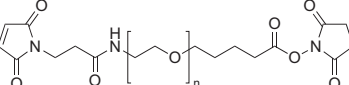
Homobifunctional PEGs

For more information on these products, visit aldrich.com/peg.

α - and ω -ends	Structure	Molecular Weight	Prod. No.
amine		average M_n 2,000	753084-1G 753084-5G
		average M_n 6,000	752444-1G 752444-5G
		average M_n 10,000	752460-1G 752460-5G
azide		average M_n 10,000	767530-1G
		average M_n 20,000	756601-1G
methacrylate		average M_n 6,000	687537-1G
		average M_n 10,000	725684-1G
		average M_n 20,000	725692-1G
NHS		average M_n 2,000	713783-500MG
		average M_n 3,000	15961-1G-F
		average M_n 10,000	713791-500MG
SH		average M_n 1,000	717142-1G
		average M_n 3,400	704539-1G
		average M_n 8,000	705004-1G

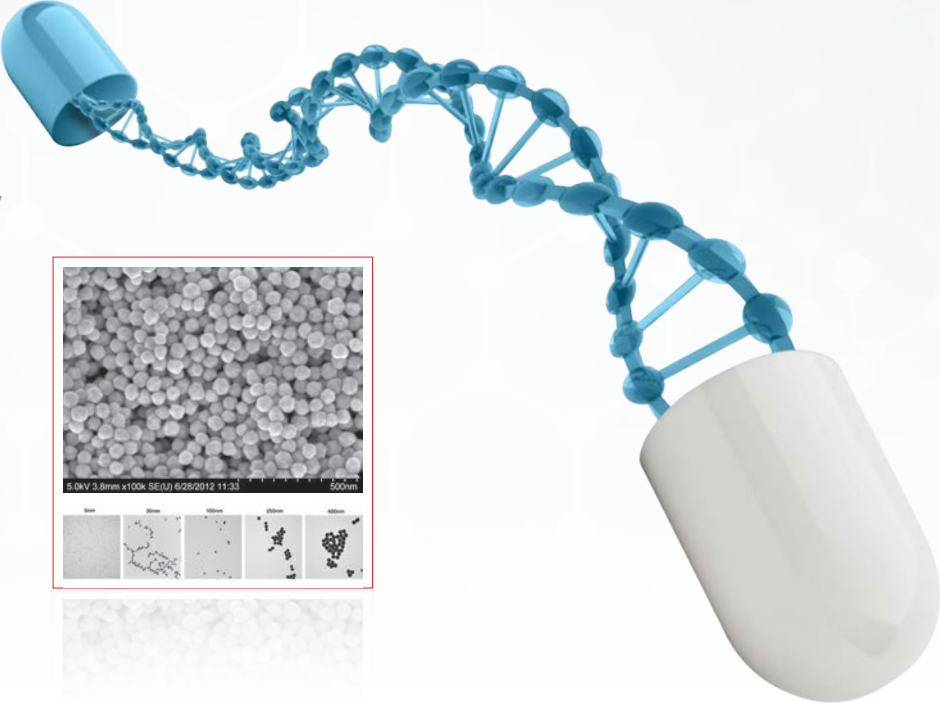
Heterobifunctional PEGs

For more information on these products, visit aldrich.com/peg.

α -end	ω -end	Structure	Molecular Weight	Prod. No.
Biotin	NHS		average M_n 3,800	757799-100MG
COOH	NH ₂		average M_n 1,100	757861-100MG
			average M_n 2,100	757888-100MG
	SH		average M_n 3,500	757896-100MG
			average M_n 1,000	757810-500MG
Maleimide	COOH		M_p 3,000	670162-250MG
	NH ₂		average M_n 4,000	757853-100MG



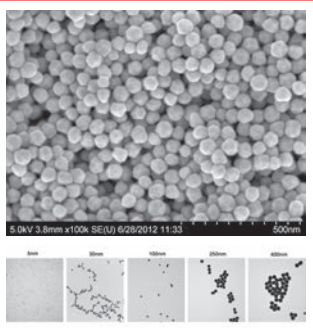
FUNCTIONALIZED, PEGYLATED GOLD NANOPARTICLES



BIOMEDICAL | ELECTRONICS | ENERGY

ENHANCE YOUR IMAGE

- End-group functionalized
 - Carboxylic acid, amino, biotin for protein conjugation
 - Methoxy for non-binding
- Nanoparticle sizes from 5 nm to 50 nm
- 3 or 5 kDa PEG lengths



aldrich.com/functionalnano

THREE-DIMENSIONAL PRINTING OF TISSUE ENGINEERING SCAFFOLDS



Helena N. Chia, Ph.D.,^{1*} Benjamin M. Wu, D.D.S., Ph.D.^{1,2*}

¹Department of Bioengineering, Henry Samueli School of Engineering
University of California, Los Angeles, CA 90095 USA

²Division of Advanced Prosthodontics, Department of Materials Science and Engineering
Department of Orthopedic Surgery, University of California, Los Angeles, CA 90095 USA

*Email: benwu@ucla.edu

Introduction

Three-dimensional printing (3DP) can be used to produce complex tissue engineering scaffolds based on computer designs obtained from patient-specific anatomical data. 3DP was first used in the biomedical field to produce pre-surgical visualization models and tooling molds. Since its first use, 3DP has evolved to enable the creation of tissue engineering scaffolds, tissue analogs, and organs-on-chip for diagnostics. Recent growth in public interest and access to affordable printers have fueled a renewed drive to combine stem cell technology with custom three-dimensional (3D) scaffolds to create the field of personalized regenerative medicine. However, there are a number of technological issues that must be addressed before 3DP can be routinely used for the regeneration of complex tissues such as bone, cartilage, muscles, blood vessels, or complex organs with intricate 3D microarchitecture such as liver or lymphoid organs. Herein, we will explore the technological advances that have contributed toward the progress of 3DP of tissue engineering scaffolds, current materials used to create 3DP scaffolds, and the challenges that remain.

Most 3DP methods use a layer-by-layer process to fabricate objects. The general 3DP process involves: 1) creating a solid 3D computer model either from medical imaging data or by computer aided design (CAD); 2) slicing the 3D model into consecutive two-dimensional (2D) slices; 3) fabricating each slice by a computer-controlled layer-by-layer process; and 4) finishing with post-processing such as surface modification to create nanoarchitecture. Using this approach, complicated 3D features such as internal voids, cantilevers, undercuts, and narrow tortuous paths are reduced to a stack of common 2D features such as circles, lines, and points. Exempted from tooling path restrictions, where material can only be removed when it is physically accessible, these additive technologies offer much higher levels in shape complexity. The ability to create these complex 3D shapes is very attractive for biomedical engineering, and various 3DP techniques have been introduced to fabricate objects that include controlled macroarchitecture and microstructures for application in biomedical and tissue engineering. Biomedical researchers are rapidly embracing 3DP because the combination of freedom in form and material deposition technology offers remarkable control over the tissue engineering triad of cells, signals, and scaffolding substrates.

The expiration of core 3DP patents and the availability of affordable computational power for the processing of massive 3D files have both contributed to the recent explosive growth of 3DP. Technological advances now enable the design and fabrication of complex 3D structures with patient-specific macro- and microarchitecture. FreeCAD open-source software and other CAD apps enable design and sharing of parts even at home. Now 3D image acquisition can be completed using low-cost, high resolution 3D scanners; apps that promise to enable 3D scanning using a smartphone are under development. The combination of these advances has propelled the popularity and accessibility of 3DP to a much larger audience. Even 3DP machines developed for consumers can be adapted for the fabrication of tissue scaffolds. The widespread availability of quality instrumentation now opens the door to address the remaining fundamental limitation of 3DP—the scarcity of implantable biomaterials for printing. In the following sections, each 3DP technology is briefly introduced and the materials they currently use will be discussed.

Powder 3D Printing

Invented at the Massachusetts Institute of Technology, powder 3D printers deposit a liquid binder solution from an inkjet onto a powder bed to fabricate 3D structures.¹⁻³ The powder 3DP process begins by spreading a layer of fine powder material evenly across the piston. The X-Y positioning system and the printhead are synchronized to print the desired 2D pattern through the selective deposition of binder droplets onto the powder layer. After printing, the piston, powder bed, and printed part are lowered, and the next layer of powder is spread (**Figure 1**).

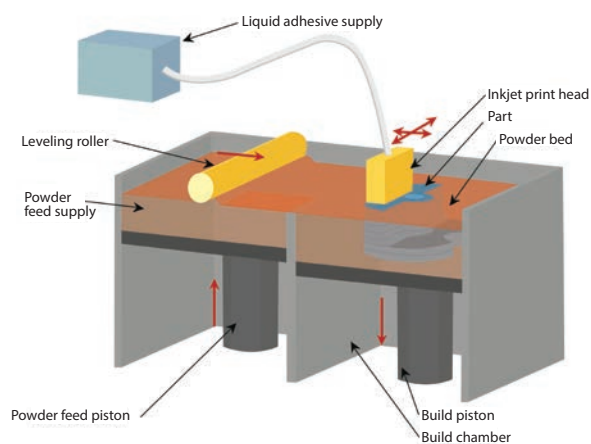


Figure 1. Illustration of powder 3D printing based on a series of steps that use a binding agent to secure powder in a 2D pattern, where the loose powder is removed after the part is printed.

The drop-spread-print cycle is repeated until the entire part is completed. Removal of the unbound powder reveals the fabricated part. Biomaterials such as peptides, proteins [e.g., fibrinogen (example **Sigma Prod. No. F3879**) and collagen], polysaccharides (e.g., hyaluronan and alginate), DNA plasmids, and living cells can be incorporated into

the binder or processed as the powder for direct 3DP. Other previously used materials include synthetic polymers [i.e., poly(ϵ -caprolactone), polylactide–glycolide or poly(L-lactic acid)] with an organic solvent as the binder and natural polymer powders [i.e., starch (**Sigma-Aldrich Prod. No. 03967**), dextran and gelatin (**Sigma Prod. No. G1890**)] with water as a binder. Currently used materials include ceramics [i.e., tricalcium phosphate, hydroxyapatite (**Aldrich Prod. No. 289396**), and calcium polyphosphate], synthetic polymers (i.e., polyvinyl alcohol, PLGA, PCL), and natural polymers [i.e., collagen and chitosan (**Aldrich Prod. Nos. 448869, 448877, and 419419**)]. To use these biomaterials, the biomaterials usually do not require special modification or functionalization, but they must be in a powder form. *In vivo* studies have been performed using these materials for the correction of bone defects (calvarial, tibia, femoral) in rabbit, rat, and mouse models.^{4–9} Alternatively, porogens such as sucrose (**Sigma Prod. No. 57903**), lactose, or table salt can be printed to create the desired shape. After polymer solutions are infused into the interstitial space, the dissolution of the porogens yields a 3D part of biopolymer.¹⁰

Fused-deposition Modeling

Fused-deposition modeling (FDM) is the deposition of molten thermoplastic materials in specific patterns using two heated extrusion heads that each include a small orifice.¹¹ One nozzle deposits the thermoplastic material and the second deposits temporary material to support cantilevers (**Figure 2**). In one traditional FDM method, thermoplastic polymer is melted into a semi-liquid state and the head extrudes this material onto the build platform. The most important material selection criteria for FDM materials are heat transfer characteristics and rheology (behavior of liquid flow). In order to allow flow of the material for specific lay-down patterns, thermoplastics are commonly selected because of their low melting temperature. PVC, nylon, ABS, and investment casting wax have also been successfully used. For bioapplications, PCL is commonly used due to its low melting temperature (~60 °C), low glass transition temperature (~60 °C), and high thermal stability. Other materials used include PLGA, TCP (combined with a synthetic polymer), PMMA (**Aldrich Prod. Nos. 200336, 182230, and 445746**), poly(ethylene glycol) terephthalate, and poly(butylene) terephthalate. Combinations of these materials are also used. This technology has been used in several *in vivo* studies, including animal models (e.g., murine animal models for wound healing and rabbit bone defects)^{12–14} and the treatment of a craniofacial defect in a human patient.¹⁵

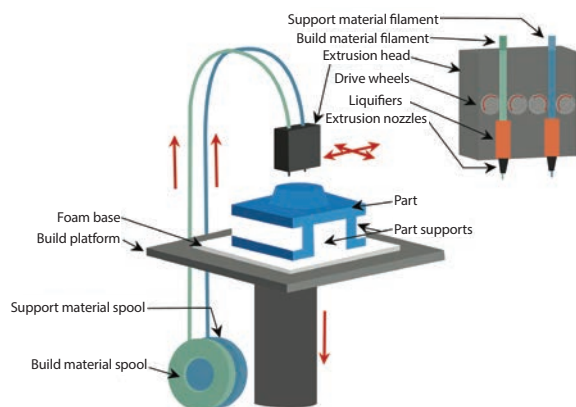


Figure 2. Illustration showing the fused-deposition modeling process, where molten thermoplastic material is deposited in specific patterns.

Stereolithography

Stereolithography (SLA) was developed in the late 1980s and is regarded as the first rapid prototyping process.¹⁶ The original SLA method uses a rastered HeCd-laser beam to spatially control the polymerization of a photocurable resin in 2D patterns.¹⁷ After each layer is cured, the platform containing the cured structure is lowered (in the bottom-up approach) and another layer of uncured liquid resin spreads over the top (**Figure 3**). The topmost layer is ready to be patterned once the resin has spread. For the top-down approach, light is projected onto a transparent plate that is initially positioned near the bottom of the vessel holding the liquid resin. The build is detached from the transparent plate for each subsequent layer. Acrylics and epoxies are typically used in SLA; any materials used for SLA must include photocurable moieties for photocrosslinking. For tissue engineering applications, very few biodegradable and biocompatible biomaterials are dimensionally stable enough during photopolymerization for use in SLA. Over the last few years, more polymers have been synthesized that contain aliphatic polyesters that allow for biodegradation. The resulting macromer is then acrylated to enable photocrosslinking, for example, in poly(ethylene glycol) diacrylate. This trend has increased the library of available resins with biodegradable moieties and the encapsulation of cells during processing. These novel macromers include segments of PCL or poly(D,L-lactide), PLLA resins with modified end groups to allow for photocrosslinking capability, and PPF-DEF. *In vivo* studies have shown these materials can promote bone formation in rat cranial defects.¹⁸

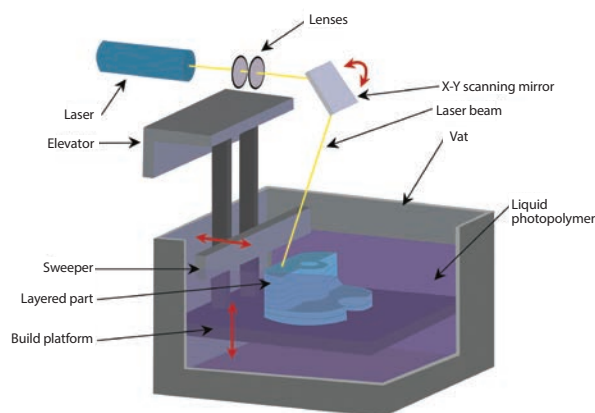


Figure 3. Illustration of the stereolithography process using layers of liquid photopolymerizable polymers.

Selective Laser Sintering

Selective laser sintering (SLS) was developed at the University of Texas in 1989.¹⁹ SLS is similar to powder 3DP in that powder particles are bound together in thin layers. In this method, however, a CO₂ laser beam is used to bond the material by sintering.²⁰ The laser scans the surface of the powdered polymer particles in a specific 2D pattern in order to sinter them above the glass transition temperature (**Figure 4**). During sintering, molecular diffusion along the outermost surface of the particle leads to neck formation between neighboring particles. After one layer is created, the piston containing the part is lowered and a fresh layer of powder material is rolled across the top surface. The subsequent layer is formed and bound to the previous layer. Unbound powder is removed after fabrication; the part is then heat-treated to achieve full density. Combinations of powders such as PCL and hyaluronic acid are commonly used. Biomedical applications of this technique include bone and vascular tissue engineering²¹ and inter-body cages for spinal fusions.²²

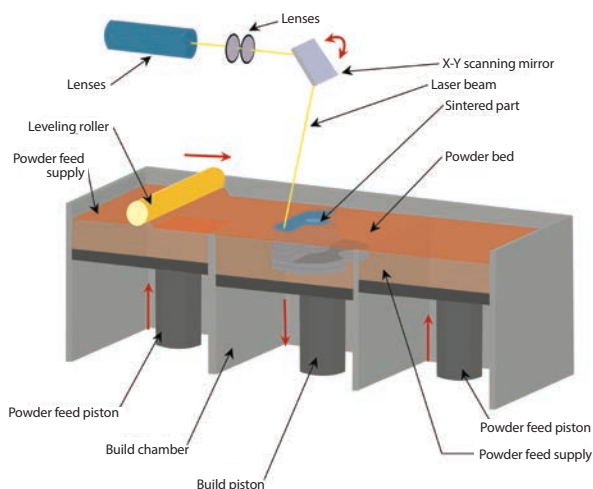


Figure 4. Illustration showing the selective laser sintering process.

Three-dimensional Plotting/Direct-write Bioprinting

Three-dimensional plotting was developed at the Freiburg Materials Research Center in 2000 to create soft tissue scaffolds. This 3D plotting is based on extruding a viscous liquid material (generally a solution, paste, or dispersion) from a pressurized syringe into a liquid medium with matching density. The material is deposited in one long continuous strand or in individual dots from a nozzle or syringe to create a desired 3D shape of ceramics, polymers, or hydrogels.²³ Similarly, bioprinting is the fabrication of hydrogel structures with direct incorporation of cells. This technology provides a controlled spatial distribution of cell or growth factors as well as the scaffold structures. Bioplotting materials include synthetic polymers and natural polymers such as collagen, chitosan, alginate, agarose, or gelatin. Most hydrogels compatible with cell bioprinting are ideal for implantation in biological environments that do not require high mechanical properties, such as cavalerial defects.²⁴ Bioprinting has also been used to develop personalized cell-based chips to evaluate patient-specific drug response and cytotoxicity.²⁵

Future Directions

Although there have been great strides in tissue engineering over the last five years, innervation and vascularization (the development of nerves and blood vessels within these tissues) of emerging tissues still remain very challenging. To achieve a fully functioning 3D-printed tissue that is integrated with the circulatory and neural control systems, functional gradients of cells and biochemical molecules must be created that mimic the conditions during embryogenesis and wound healing. Further, the deposition of cells requires materials and processing conditions that are

fully compatible with biomaterials, unlike processing conditions with UV light, heat, organic solvents, or cytotoxic photoinitiators, among others. Incorporation of biochemical molecules necessitates the development of sustained growth factor release in controlled spatial-temporal release profiles. The creativity that now drives 3DP must be directed toward addressing these challenges in order for the field to evolve.

The outlook on 3DP for tissue engineering is extremely exciting. Technological advancements have made 3DP more accessible to those outside of industry and academia and allowed for more robust design and fabrication of scaffolds. New materials and methods are continuously being made to expand the applications of biocompatible scaffolds, such as using DNA sequences to place different types of cells in 3D to create organoid-like tissues (DNA-programmed assembly of cells or DPAC).²⁶ This convergence is ideal to accelerate 3DP development to create the next generation tissue engineering structures.

References

- (1) Cima, M. J.; Sachs, E.; Cima, L. G.; Yoo, J.; Khanuja, S.; Borland, S. W.; Wu, B.; Giordano, R. A. In *Solid Freeform Fabr. Symp. Proc.*; DTIC Document, **1994**; pp 181–190.
- (2) Griffith, L. G.; Wu, B.; Cima, M. J.; Powers, M. J.; Chaignaud, B.; Vacanti, J. P. *Ann. N. Y. Acad. Sci.* **1997**, *831* (1), 382–397.
- (3) Wu, B. M.; Borland, S. W.; Giordano, R. A.; Cima, L. G.; Sachs, E. M.; Cima, M. J. *J. Controlled Release* **1996**, *40* (1), 77–87.
- (4) Abarrategi, A.; Moreno-Vicente, C.; Martínez-Vázquez, F. J.; Civantos, A.; Ramos, V.; Sanz-Casado, J. V.; Martínez-Corria, R.; Perera, F. H.; Mulero, F.; Miranda, P. *PLoS One* **2012**, *7* (3), e34117.
- (5) Tamimi, F.; Torres, J.; Gbureck, U.; Lopez-Cabarcos, E.; Bassett, D. C.; Alkhrasat, M. H.; Barralet, J. E. *Biomaterials* **2009**, *30* (31), 6318–6326.
- (6) Tarafder, S.; Dernel, W. S.; Bandyopadhyay, A.; Bose, S. *J. Biomed. Mater. Res. Part B Appl. Biomater.* **2014**, *103* (3), 679–690.
- (7) Tarafder, S.; Balla, V. K.; Davies, N. M.; Bandyopadhyay, A.; Bose, S. *J. Tissue Eng. Regen. Med.* **2013**, *7* (8), 631–641.
- (8) Tarafder, S.; Davies, N. M.; Bandyopadhyay, A.; Bose, S. *Biomater. Sci.* **2013**, *1* (12), 1250–1259.
- (9) Inzana, J. A.; Olvera, D.; Fuller, S. M.; Kelly, J. P.; Graeve, O. A.; Schwarz, E. M.; Kates, S. L.; Awad, H. A. *Biomaterials* **2014**, *35* (13), 4026–4034.
- (10) Chia, H. N.; Wu, B. M. *J. Biomed. Mater. Res. Part B Appl. Biomater.* **2014**, n/a – n/a.
- (11) Zein, I.; Huttmacher, D. W.; Tan, K. C.; Teoh, S. H. *Biomaterials* **2002**, *23* (4), 1169–1185.
- (12) Teo, E. Y.; Ong, S.-Y.; Khoon Chong, M. S.; Zhang, Z.; Lu, J.; Mochhala, S.; Ho, B.; Teoh, S.-H. *Biomaterials* **2011**, *32* (1), 279–287.
- (13) Kim, J.; McBride, S.; Tellis, B.; Alvarez-Urena, P.; Song, Y.-H.; Dean, D. D.; Sylvia, V. L.; Elgendy, H.; Ong, J.; Hollinger, J. O. *Biofabrication* **2012**, *4* (2), 25003.
- (14) Shim, J.-H.; Moon, T.-S.; Yun, M.-J.; Jeon, Y.-C.; Jeong, C.-M.; Cho, D.-W.; Huh, J.-B. *J. Mater. Sci. Mater. Med.* **2012**, *23* (12), 2993–3002.
- (15) Probst, F. A.; Huttmacher, D. W.; Müller, D. F.; Machens, H. G.; Schantz, J. T. *Nerven und Gefässe Organ der V.* **2010**, *42* (6), 369–373.
- (16) Dowler, C. A. *Plast. Eng* **1989**, *45* (4), 43–45.
- (17) Fisher, J. P.; Dean, D.; Mikos, A. G. *Biomaterials* **2002**, *23* (22), 4333–4343.
- (18) Lee, J. W.; Kang, K. S.; Lee, S. H.; Kim, J.-Y.; Lee, B.-K.; Cho, D.-W. *Biomaterials* **2011**, *32* (3), 744–752.
- (19) Marcus, H. L.; Beaman, J. J.; Barlow, J. W.; Boarell, D. L. *JOM* **1990**, *42* (4), 8.
- (20) Pattanayak, D. K.; Fukuda, A.; Matsushita, T.; Takemoto, M.; Fujibayashi, S.; Sasaki, K.; Nishida, N.; Nakamura, T.; Kokubo, T. *Acta Biomater.* **2011**, *7* (3), 1398–1406.
- (21) Liao, H.; Lee, M.; Tsai, W.; Wang, H.; Lu, W. *J. Tissue Eng. Regen. Med.* **2013**.
- (22) Kang, H.; Hollister, S. J.; La Marca, F.; Park, P.; Lin, C.-Y. *J. Biomech. Eng.* **2013**, *135* (10), 101013.
- (23) Landers, R.; Mülhaupt, R. *Macromol. Mater. Eng.* **2000**, *282* (1), 17–21.
- (24) Haberstroh, K.; Ritter, K.; Kuschnier, J.; Bormann, K.; Kaps, C.; Carvalho, C.; Mülhaupt, R.; Sittinger, M.; Gellrich, N. *J. Biomed. Mater. Res. Part B Appl. Biomater.* **2010**, *93* (2), 520–530.
- (25) Xu, F.; Wu, J.; Wang, S.; Durmus, N. G.; Gurkan, U. A.; Demirci, U. *Biofabrication* **2011**, *3* (3), 034101.
- (26) Todhunter, M.; Jee, N.; Hughes, A.; Coyle, M.; Cerchiari, A.; Farlow, J.; Garbe, J.; LaBarge, M.; Desai, T.; Gartner, Z. *Nature methods* **2015**.

Synthetic Polymers for 3D Printing

Polycaprolactones

For more information on these products, visit aldrich.com/polycaprolactone.

Name	Structure	Molecular Weight	Transition Temperature	Prod. No.
Polycaprolactone		average M_n ~10,000	T_g -60 °C	440752-5G 440752-250G 440752-500G
		average M_n 45,000	-	704105-100G 704105-500G
		average M_n 80,000	-	440744-5G 440744-250G 440744-500G
Polycaprolactone dimethacrylate		average M_n 550	-	802115-2G
		average M_n 2,250	-	802158-2G
Polycaprolactone diol		average M_n ~530	softening point 35 °C	189405-250G 189405-500G
		average M_n ~2,000	softening point 50 °C	189421-250G 189421-500G
Polycaprolactone trimethacrylate		average M_n 950	-	799556-2G
Polycaprolactone triol		average M_n ~300	softening point 10 °C	200387-250G 200387-500G
		average M_n ~900	softening point 30 °C	200409-250G 200409-500G

Block PCL Polymers

For more information on these products, visit aldrich.com/polycaprolactone.

Name	Structure	Composition	Inherent Viscosity	Transition Temperature	Prod. No.
Poly(DL-lactide-co-caprolactone)		DL-lactide 86 mol %	0.7-0.9 dL/g in chloroform	T_g 16 °C	457647-5G
		DL-lactide 40 mol %	0.7-0.9 dL/g in chloroform	T_m 31 °C, DSC, onset	457639-5G
Poly(L-lactide-co-caprolactone-co-glycolide)		glycolide 10% L-lactide 70% caprolactone 20%	-	-	568562-1G 568562-5G

ABS 3D Printing Filaments

For more information on these products, visit aldrich.com/absfilaments.

Color	Diameter	Prod. No.
black	1.75 mm	3DXABS001-1EA
	2.85 mm	3DXABS002-1EA
blue	1.75 mm	3DXABS003-1EA
	2.85 mm	3DXABS004-1EA
green	1.75 mm	3DXABS005-1EA
	2.85 mm	3DXABS006-1EA
natural	1.75 mm	3DXABS007-1EA
	2.85 mm	3DXABS008-1EA
orange	1.75 mm	3DXABS009-1EA
	2.85 mm	3DXABS010-1EA
red	1.75 mm	3DXABS011-1EA
	2.85 mm	3DXABS012-1EA
white	1.75 mm	3DXABS013-1EA
	2.85 mm	3DXABS014-1EA
yellow	1.75 mm	3DXABS015-1EA
	2.85 mm	3DXABS016-1EA

PLA 3D Printing Filaments

For more information on these products, visit aldrich.com/plafilaments.

Color	Diameter	Prod. No.
black	1.75 mm	3DXPLA001-1EA
	2.85 mm	3DXPLA002-1EA
blue	1.75 mm	3DXPLA003-1EA
	2.85 mm	3DXPLA004-1EA
green	1.75 mm	3DXPLA005-1EA
	2.85 mm	3DXPLA006-1EA
natural	1.75 mm	3DXPLA007-1EA
	2.85 mm	3DXPLA008-1EA
orange	1.75 mm	3DXPLA009-1EA
	2.85 mm	3DXPLA010-1EA
red	1.75 mm	3DXPLA011-1EA
	2.85 mm	3DXPLA012-1EA
white	1.75 mm	3DXPLA013-1EA
	2.85 mm	3DXPLA014-1EA
yellow	1.75 mm	3DXPLA015-1EA
	2.85 mm	3DXPLA016-1EA

Biodegradable Polymers

Poly(lactide-co-glycolide) Copolymers

For more information on these products, visit aldrich.com/biopoly.

Name	Feed Ratio	End Group	Molecular Weight	Degradation Time (months)	Prod. No.
Resomer® RG 502 H, Poly(D,L-lactide-co-glycolide)	lactide:glycolide 50:50	acid terminated	M _w 7,000-17,000	<3	719897-1G 719897-5G
Resomer® RG 503 H, Poly(D,L-lactide-co-glycolide)		acid terminated	M _w 24,000-38,000	<3	719870-1G 719870-5G
Resomer® RG 504 H, Poly(D,L-lactide-co-glycolide)		acid terminated	M _w 38,000-54,000	<3	719900-1G 719900-5G
Resomer® RG 502, Poly(D,L-Lactide-co-Glycolide)		ester terminated	M _w 7,000-17,000	<3	719889-1G 719889-5G
Resomer® RG 503, Poly(D,L-lactide-co-glycolide)		ester terminated	M _w 24,000-38,000	<3	739952-1G 739952-5G
Resomer® RG 504, Poly(D,L-lactide-co-glycolide)		ester terminated	M _w 38,000-54,000	<3	739944-1G 739944-5G
Resomer® RG 505, Poly(D,L-lactide-co-glycolide)		ester terminated	M _w 54,000-69,000	<3	739960-1G 739960-5G
Resomer® RG 653 H, Poly(D,L-lactide-co-glycolide)	lactide:glycolide 65:35	acid terminated	M _w 24,000-38,000	<5	719862-1G 719862-5G
Resomer® RG 752 H, Poly(D,L-lactide-co-glycolide)	lactide:glycolide 75:25	acid terminated	M _w 4,000-15,000	<6	719919-1G 719919-5G
Resomer® RG 756 S, Poly(D,L-lactide-co-glycolide)		ester terminated	M _w 76,000-115,000	<6	719927-1G 719927-5G
Poly(D,L-lactide-co-glycolide)	lactide:glycolide 85:15	ester terminated	M _w 50,000-75,000	<6	430471-1G 430471-5G
Resomer® RG 858 S, Poly(D,L-lactide-co-glycolide)		ester terminated	M _w 190,000-240,000	<9	739979-1G 739979-5G

Well-defined Poly(L-lactide)s

For more information on these products, visit aldrich.com/biopoly.

Name	Molecular Weight (M _n)	PDI	Degradation Time (years)	Prod. No.
Poly(L-lactide)	5,000	≤ 1.2	>3	764590-5G
	10,000	≤ 1.1	>3	765112-5G
	20,000	≤ 1.1	>3	764698-5G

Well-defined Poly(D,L-lactide)s

For more information on these products, visit aldrich.com/biopoly.

Name	Molecular Weight (M_n)	PDI	Degradation Time (months)	Prod. No.
Poly(D,L-lactide)	5,000	≤ 1.1	<6	764612-5G
	10,000	≤ 1.1	<6	764620-5G
	20,000	≤ 1.3	<6	767344-5G

Poly(L-lactide)s

For more information on these products, visit aldrich.com/biopoly.



Name	End Group	Molecular Weight	Degradation Time (years)	Prod. No.
Resomer® L 206 S, Poly(L-lactide), ester terminated	ester terminated	-	>3	719854-5G 719854-25G
Poly(L-lactide)	ester terminated	average M_n 50,000	>3	94829-1G-F 94829-5G-F
	ester terminated	M_n 59,000 M_w 101,000	>3	93578-5G-F
	ester terminated	M_w ~260,000	>3	81273-10G
	ester terminated	M_n 103,000 M_w 259,000	>3	95468-1G-F 95468-5G-F

Poly(D,L-lactide)s

For more information on these products, visit aldrich.com/biopoly.



Name	End Group	Molecular Weight	Degradation Time (months)	Prod. No.
Resomer® R 202 H, Poly(D,L-lactide)	acid terminated	M_w 10,000-18,000	<6	719978-1G 719978-5G
Resomer® R 203 H, Poly(D,L-lactide)	acid terminated	M_w 18,000-24,000	<6	719943-1G 719943-5G
Resomer® R 202 S, Poly(D,L-lactide)	ester terminated	M_w 10,000-18,000	<6	719951-1G 719951-5G
Resomer® R 203 S, Poly(D,L-lactide)	ester terminated	M_w 18,000-28,000	<6	719935-1G 719935-5G

End-functionalized Low PDI Poly(L-lactide)

For more information on these products, visit aldrich.com/biopoly.

Name	Structure	Molecular Weight	PDI	Prod. No.
Poly(L-lactide), acrylate terminated		average M_n 2,500	≤ 1.2	775991-1G
		average M_n 5,500	≤ 1.2	775983-1G
Poly(L-lactide), amine terminated		average M_n 2,500	≤ 1.3	776378-1G 776378-5G
		average M_n 4,000	≤ 1.2	776386-1G 776386-5G
		average M_n 5,000	< 1.2	774146-1G
Poly(L-lactide), N-2-hydroxyethylmaleimide terminated		average M_n 2,000	≤ 1.2	746797-1G 746797-5G
		average M_n 5,000	< 1.2	746517-1G 746517-5G
Poly(L-lactide), 2-hydroxyethyl, methacrylate terminated		average M_n 2,000	≤ 1.1	771473-1G 771473-5G
		average M_n 5,500	≤ 1.2	766577-1G 766577-5G
Poly(L-lactide), propargyl terminated		average M_n 2,000	≤ 1.1	774162-1G
		average M_n 5,000	≤ 1.1	774154-1G
Poly(L-lactide), thiol terminated		average M_n 2,500	≤ 1.2	747386-1G 747386-5G
		average M_n 5,000	≤ 1.2	747394-1G 747394-5G

TAILORING COLLAGEN-BASED MATRICES FOR REGENERATIVE MEDICINE AND TISSUE ENGINEERING



Jiayu Leong,¹ Liam Grover,² Hyunjoon Kong^{1*}

¹Department of Chemical and Biomolecular Engineering
University of Illinois, Urbana-Champaign, IL 61801 USA

²University of Birmingham, UK

*Email: hjkong06@illinois.edu

Introduction

Collagen molecules play a critical role in tissue architecture and strength, and in cell-matrix interactions as insoluble ligands to regulate the diverse phenotypic activities of cells. Whether isolated from animal tissue or produced via recombinant techniques, the enzyme-mediated biodegradability and cell adhesion properties of collagen position it as a promising building block for matrices used in both fundamental and applied bioscience. Additionally, studies have shown that collagen elicits very low immunogenicity, making it a suitable platform for the development of therapies that include long-term cell transplantation in the body, such as tissue regeneration. Efforts to further improve the performance of collagen-based materials for use in tissue engineering include the modulation of biomolecular, chemical, and mechanical characteristics using a variety of chemical conjugation and physical association techniques. For example, collagen-based materials processed in the form of gels and microporous matrices have been chemically modified to present bioactive molecules that regulate the phenotypic and secretion activities of cells of interests. In addition, the microstructure of collagen-based materials has been chemically and physically engineered to modulate its mechanical and transport properties. Through these efforts, extensive progress has been made in engineering three-dimensional (3D) collagen scaffolds into functional materials that have the potential to promote the restoration of tissues *in vitro* and *in vivo*. Here we summarize a series of recent chemical modifications and processes used to engineer a collagen-based matrix capable of improving therapeutic efficacies of regenerative medicine for the treatment of various tissue defects.

Variance of Isolated Collagen

Collagens make up a large group of triple-helical proteins that comprise the most abundant protein family found in vertebrates, representing about 30% of total proteins. In general, an individual collagen polypeptide chain has a large number of repeating amino acid sequences, most often glycine-X-Y, where X is proline and Y is hydroxyproline. Type I collagen, the most abundant in the human body, contains 31–38 lysine residues in each chain.¹ Interestingly, the number and sites of lysine residues in the collagen molecule are highly conserved between human, mouse, rat, and bovine species. This small difference in amino acid composition between different species results in minimal clinical immunogenicity for medical applications, including cosmetic dermal fillers and wound healing dressings. One important source of variation among different types of collagen is the modification of lysine residues to form hydroxylysine. Hydroxylation of prolines and lysines has a significant effect on collagen fibrillogenesis and matrix mineralization.² While the differences in hydroxylation patterns are essential in the formation of characteristic connective tissues in various parts of the body, these differences will affect the structural and chemical properties of the scaffold to be used for tissue engineering. For this reason, it is important to identify the source and the chemical composition of naturally derived collagen for reliable and reproducible engineering of collagen-based materials.

Recombinant Synthesis of Collagen

To circumvent the impact of the variability of naturally derived collagen on the properties and functions of materials, recombinant techniques to manufacture homogeneous collagen are increasingly being used. Recombinant collagen molecules are produced through the transfection of mammalian cells, insect cells, yeast, or *Escherichia coli* with gene encoding collagen molecules. Recombinant collagens will self-assemble into ordered fibrous structures similar to that of naturally derived collagen.³ For instance, hydrogels fabricated by crosslinking recombinant human collagen type III (made in the yeast *Pichia pastoris*) demonstrate a comparable glucose diffusion coefficient with that of human corneal stroma.⁴

Recombinant techniques also have been used to introduce non-native cysteines for bioconjugation via sulfhydryl chemistry. This is particularly useful for collagen engineering because cysteines do not naturally occur within the triple-helical region of native collagen. The fabrication of recombinant human collagen containing 2, 4, or 8 non-native cysteines at precisely defined locations within each biopolymer has expanded the capability of collagen engineering by allowing the use of sulfhydryl chemistry to form hydrogels and immobilize bioactive factors. It is important to note collagen variants that include non-native cysteines more robustly retain their triple-helical structure and support cellular adhesion.⁵

Coupling Biomolecules to Collagen-based Materials

Collagen molecules have been designed to form porous scaffolds, gels, fibers, and films to direct cells in the reconstruction of damaged tissues. Additionally, collagen can be used to encapsulate and engineer cells within a matrix to elicit regenerative functions at an injured site upon transplantation. The biochemical composition and mechanical properties of the scaffold not only impact the viability and phenotype of the encapsulated cells, but also influence the function and structural characteristics of the collective cell population. The characteristics of the matrix can be tuned and customized for a specific therapeutic application by a variety of methods. For example, immobilized growth factors can be used to provide bioactive cues that enhance cellular attachment and growth of functional tissues. In addition, matrix stiffness can be controlled to instruct cells to follow different fates.

A number of chemical strategies can be used to couple collagen with molecules of interest. The primary ϵ -amino group of lysines on collagen is particularly reactive towards compounds containing isothiocyanates, isocyanates, *N*-hydroxysuccinimide esters (NHS), pentafluoroesters, aldehydes, or activated carboxyl groups. Since lingering by-products and unreacted crosslinkers can be internalized and react with other proteins found in the cells, it is important to select reagents that do not cause potential toxicities. For instance, glutaraldehyde (Sigma-Aldrich Prod. No. 3802) is an aggressive carbonyl reagent that condenses amines

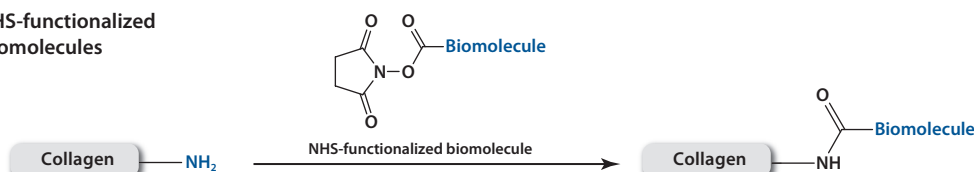
via Mannich reactions and/or reductive amination. However, without thorough purification, unreacted glutaraldehyde can have toxic effects because it may cause proteins in cells and tissues to crosslink.^{6,7}

NHS esters are frequently used for the specific functionalization of biomolecules onto amino groups on collagen molecules (Scheme 1A). A wide variety of commercially produced NHS-functionalized biomolecular probes for protein labeling are now available. Conversely, aspartic and glutamic acids may be used as the anchoring groups to react with amino-functionalized biomolecules. To improve reactivity, carbodiimides, such as 1-ethyl-3-(3-dimethylaminopropyl)carbodiimide (EDC) (Aldrich Prod. No. 39391), are often used together with water-soluble sulfo-NHS (Aldrich Prod. No. 56485) to activate the carboxyl groups (Scheme 1B). For instance, Hosseinkhani et al. chemically modified collagen with a laminin-mimicking pentapeptide epitope consisting of isoleucine-lysine-valine-alanine-valine (IKVAV). Compared with a matrix of unmodified collagen, a matrix assembled with the IKVAV-coupled collagen significantly enhances the capability of dorsal root ganglion cells to form neural networks *in vitro*.⁸ In addition, EDC/NHS ester chemistry is advantageous for coupling folded proteins to collagen while retaining the original protein conformation and bioactivity. For example, the signaling protein, vascular endothelial growth factor (VEGF), immobilized onto a collagen matrix using EDC/NHS chemistry greatly increases the viability of endothelial cells cultured in the matrix relative to VEGF in solution.⁹

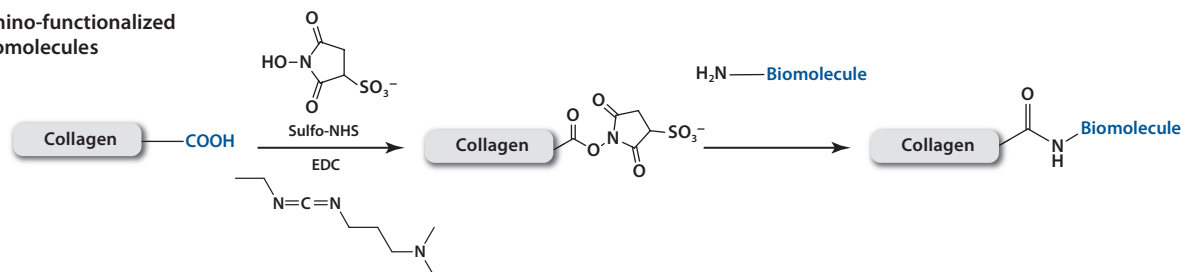
Alternatively, Traut's reagent, also known as 2-iminothiolane (Sigma Prod. No. I6256), is a small thiolation compound that reacts with primary amines to add a small spacer arm terminated by a free sulfhydryl group

Collagen conjugation with:

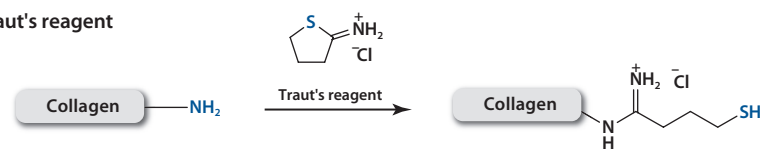
A) NHS-functionalized biomolecules



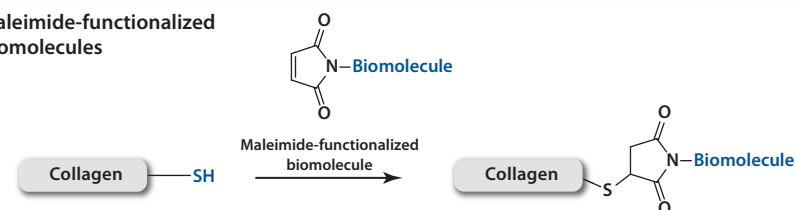
B) Amino-functionalized biomolecules



C) Traut's reagent



D) Maleimide-functionalized biomolecules



Scheme 1. Conjugation methods to functionalize collagen with A) NHS-functionalized biomolecules; B) amino-functionalized biomolecules; C) sulfhydryl group via Traut's reagent; or D) maleimide-functionalized biomolecules.

(Scheme 1C). Using this reagent, thiol-containing biomolecules can be attached to collagen through the formation of reversible disulfide bonds while maleimide-containing biomolecules can be attached via stable thioether bonds. Maleimide groups can be introduced onto peptides or proteins through sulfo-SMCC (sulfosuccinimidyl 4-(*N*-maleimidomethyl) cyclohexane-1-carboxylate) (Sigma-Aldrich Prod. No. M6035) (Scheme 1D). Bone morphogenetic protein-2 (BMP2) is required to induce osteogenic differentiation of host or transplanted mesenchymal stem cells for enhanced bone tissue regeneration. In order to achieve controlled release of BMP2, poly-histidine antibodies modified with sulfo-SMCC were conjugated to a collagen matrix using Traut's reagent.¹⁰ More poly-histidine antibodies were conjugated on collagen through the chemical crosslinking than by physical adsorption, thus resulting in a collagen system that releases poly-histidine-tagged BMP2 over an extended time period. As a consequence, the engineered collagen matrix facilitated growth of viable and functional osteoblasts.

This approach was extended to simultaneously immobilize thiol-containing biomolecules and induce crosslinking between collagen fibers in order to reduce the collagen degradation rate.¹¹ It was demonstrated that crosslinking between internal sulfhydryl groups leads to slower degradation of the collagen matrices and moderately increases revascularization. Additionally, revascularization was further increased by immobilizing VEGF via disulfide linkages due to the sustained presence of the protein on the scaffold.

In order to gain greater spatial control, biomolecules can also be coupled to a collagen matrix in a pre-defined micropattern using benzophenone-4-isothiocyanate and exposure to irradiation.^{12,13} Upon excitation with UV light, benzophenone forms a transient diradical that reacts with nearby C–H bonds from an adjacent biomolecule, forming a C–C covalent bond between the biomolecule and the matrix surface.

The aforementioned conjugation methods are limited to surface modifications because molecular diffusion prevents the penetration of the bulk material. In an effort to incorporate peptides into the bulk, Duan et al. conjugated target peptides onto amine-terminated polypropylene dendrimers.¹⁴ The remaining amine groups on the dendrimer were used as collagen crosslinkers through the chemical reaction of aspartic acids and glutamic acids in collagen (Scheme 1B), thereby incorporating the peptide into the bulk structure of the gel. Using this method, the amount of peptide can be controlled by varying the amount of peptide reacted with the dendrimer or the amount of modified dendrimer used in the

collagen gel crosslinking reaction. Using YIGSR, a laminin-derived cell adhesion peptide, we showed both surface and bulk modification of collagen matrices using YIGSR peptides lead to improved adhesion and proliferation of human corneal epithelial cells as well as neurite extension from dorsal root ganglia.

Physical Association of Recombinant Proteins Fused with Collagen-binding Domains

Biomolecules also interact with each other through electrostatic and van der Waals forces. These interactions can be used in scenarios where chemical modifications are not possible or desirable, particularly for immobilizing functional proteins or cells. However, external environments can strongly affect these physical associations. For instance, biomolecules bound by electrostatic attraction may be readily influenced by increased ionic strength, decreased pH, or competing counter ions. On the other hand, interactions between charged, hydrogen-bonding, or hydrophobic groups when maximized, form strong non-covalent complexes. The avidin-biotin complex is one example of an extremely strong non-covalent association. Recombinant protein techniques have been used to incorporate specific sequences of amino acids that are able to associate strongly with their counterparts. Dai et al. found that a heptapeptide containing the TKKTLRT sequence binds stably with collagen, independent of the external environment. Upon this finding, several therapeutic proteins were engineered to associate specifically with collagen by incorporating the TKKTLRT sequence into the proteins during DNA recombination.^{15,16} For instance, the collagen-binding domain (CBD)-fused brain-derived neurotrophic factor (BDNF) was incorporated into collagen scaffolds; thus, sustainably stimulating cells to develop neuronal tissue such as axons.¹⁷ The CBD-fused platelet-derived growth factor-BB can also be immobilized on collagen membranes, leading to enhanced re-epithelialization of dermal ulcer wounds, deposition of the collagen, and formation of capillary lumens within the newly formed tissue area¹⁸ Most recently, the group reported that collagen scaffolds modified with CBD-VEGF could promote urethral tissue regeneration and improve the function of the neo-urethra in a beagle extensive urethral defect model (Figure 1).¹⁹

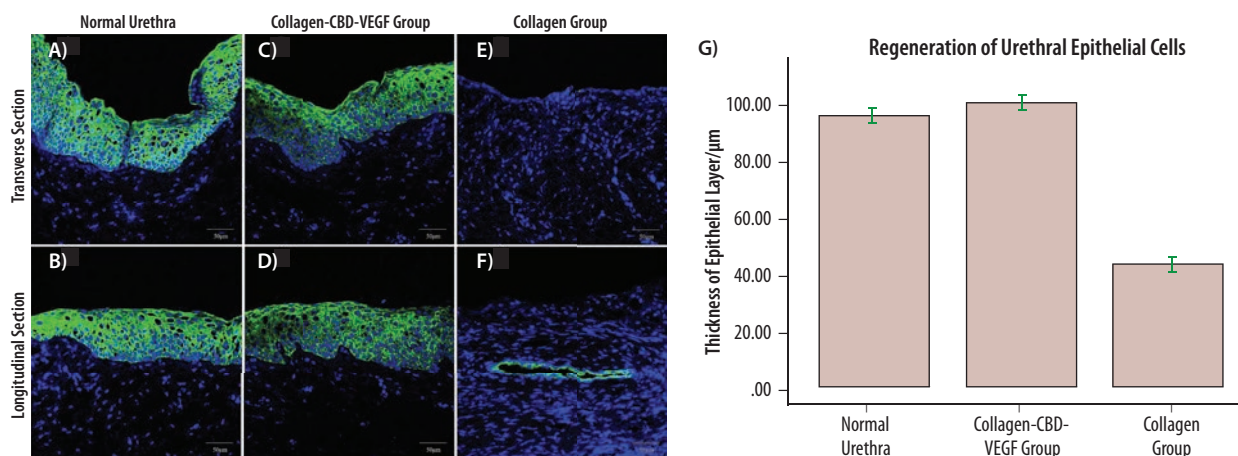


Figure 1. Immunofluorescence staining of the normal urethra (A,B) and neo-urethra at 6 months after urethral reconstruction (C,D,E,F) with mouse monoclonal antibodies against pan-cytokeratin antibody (ab86734). The epithelium covered the total segment of neo-urethra, and the mean thickness of the epithelial layer was similar to normal urethra in the collagen-CBD-VEGF group (C,D). However, the neo-urethra was not covered by a complete epithelial layer at the central section of the neo-urethra, and fistulas were generally observed in the collagen group (E,F). The mean thickness of the epithelial layer in the collagen-CBD-VEGF group was significantly larger than that in collagen group (G). Adapted from Reference 19.

Besides proteins, cells can be temporarily immobilized on collagen scaffolds through an antigen-antibody association. This strategy can be used if the antibodies for cell-specific antigens are known and easily isolated. For instance, Sca-1 positive stem cells were captured in collagen gels functionalized with the anti-Sca-1 monoclonal antibody.²⁰ When this functional collagen scaffold was transplanted into a C57/BL6 mouse as a patch to repair a surgical heart defect, enhanced regeneration of cardiomyocytes was observed.

Altering the net charge of collagen also leads to changes in the structure and association of biomolecules to collagen. Specifically, deamination, methylation, and amination have been used to modify the chemical nature of collagen prior to fabrication of collagen-glycosaminoglycan (GAG) co-precipitate.²¹ Deamination replaces the positive charges of the protonated ϵ -amino group of lysine and hydroxylysine with a neutral hydroxyl group. On the other hand, carboxyl groups of aspartic acid and glutamic acid residues in the collagen can be modified via methylation and amination. Methylation esterifies the carboxyl groups which, in turn, raise the isoelectric point. Conversely, amination converts the negatively charged carboxyl groups to positively charged amino groups and increases the cationic charge density of collagen. Since GAGs are negatively charged, the amount of GAGs retained after 6 days was found to be the highest in aminated collagen (60%) followed by methylated collagen (40%). In contrast, most GAGs were lost in the untreated group and the deaminated group within a day.

Additionally, the net charge of collagen influences intermolecular self-assembly and fibrous morphology of the matrix.²¹ Deaminated collagen forms thick fibers with large mesh size and few granules, while aminated collagen forms thin fibers with small mesh size and abundant granules, similar to the ultrastructure of the matrix in native rabbit nucleus pulposus. While the three chemically modified collagen scaffolds are equally able to support survival of human mesenchymal stem cells (MSCs), cells grown on aminated collagen have been shown to express little integrin α_v . It is speculated that the interactions between GAGs and aminated collagen might mask the ECM binding sites for integrin α_v .

These examples indicate that the sustained presence of biochemical signals has significant effect on cellular behavior. Still, another major aspect to forming effective tissue engineering scaffolds is the mechanical properties of the collagen matrices.

Tuning Mechanical Properties of Collagen Matrices

Efforts have also been made to modulate the mechanical stiffness of collagen-based materials in order to retain structural integrity and further regulate the biological activity of cells transplanted for tissue regeneration. In the past, the amount of crosslinking between collagen molecules was typically altered using cytotoxic cyanuric chloride (Aldrich Prod. No. C95501).²² Now, the elastic modulus of a collagen gel can be controlled under non-toxic conditions using a series of amine-reactive PEG derivatives such as poly(ethylene glycol) di-(succinic acid *N*-hydroxysuccinimidyl ester) (Aldrich Prod. No. 713783). Varying the amount of PEG in collagen-based hydrogels can be used to tune the stiffness of the collagen gel.^{23,24} The different collagen gel stiffness affects adhesion and phenotype of cells loaded in a collagen gel (Figure 2).

Non-reactive PEG chains incorporated in a collagen gel can be used to modulate mechanical stiffness and the diameter of individual collagen fibers by increasing the number of bound water molecules.²⁵ In particular, collagen gels become softer with increasing concentrations of PEG. The diameter of collagen fibers also increases with the concentration of PEG chains, thus recapitulating large perimysial collagen cables. Fibroblast cells cultured in the collagen-PEG gel have been shown to be responsive to the diameter of collagen fibers and form large cell bundles with extensive cell-cell contact, characteristic of the contractile proto-myofibroblast found in wound healing.

Another approach to tuning collagen gel stiffness is to introduce interpenetrating networks (IPN) using polymers that present methacrylate groups. For instance, collagen-containing poloxamine hydrogels were prepared using a four-arm PEO-PPO block copolymer (poloxamine, Tetronic®) in order to create gels that present methacrylate groups. The free radical crosslinking reaction of the polymer within pre-formed collagen gels leads to a sharp increase in stiffness compared to pure collagen gels.²⁶ Another example of an IPN gel is a network of collagen fibers crosslinked with polyacrylamide (PAAm) (Aldrich Prod. No. 749222) networks. This gel is prepared by inducing a Michael reaction between the amine groups of collagen and the vinyl groups of acrylamide. The resulting collagen fibers are chemically connected to the PAAm gel

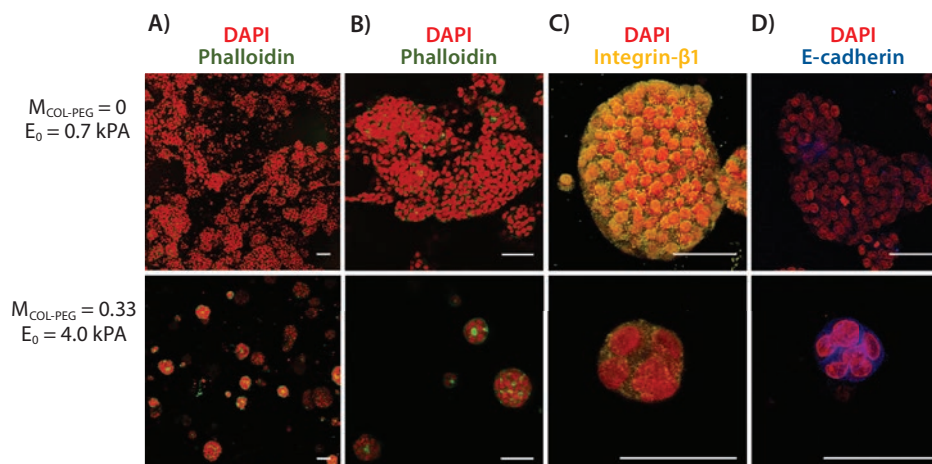


Figure 2. Effects of hydrogel elastic modulus E_0 on proliferation of 3D hepatocarcinoma spheroids. **A,B)** Spheroids formed within the pure collagen gel ($E_0 = 9.7$ kPa; 1st row) were larger and more disorganized than those formed within the collagen-PEG gels ($E_0 = 4.0$ kPa; 2nd row). Intracellular actins were stained with phalloidin (green), and the nuclei were stained with DAPI (red). Images in **B)** are magnified views of spheroids shown in **A)**. **C)** Spheroids grown in the pure collagen gel displayed higher integrin expression (yellow) than those grown in the collagen-PEG gel. Cell nuclei were stained with DAPI (red). **D)** Spheroids grown in the collagen-PEG gel expressed higher levels of E-cadherin (blue) compared to those grown in the pure collagen gel. Cell nuclei were stained with DAPI (red). Scale bars represent 50 μ m. Adapted from Reference 23.

without interfering with the crosslinking reaction between PAAm. One interesting observation is that the resulting IPN gel system enables control of the elastic modulus without significantly altering the degree of gel swelling.²⁷ The advantage of the decoupled control in these two parameters is that the gel loaded with cells or drug molecules is able to retain its structural integrity and at the same time is permeable to biomolecular transport. This is unlike other gels where there is typically an inverse dependence between water permeability and stiffness. As a result, in a sufficiently rigid matrix there is a compromise between cell viability and therapeutic availability.

Conversely, semi-IPNs (in which only collagen is three-dimensionally associated via physical crosslinking and secondary polymer chains are entangled with the collagen gel network) form less dense gels with lower storage modulus and higher degradation rate. With these differences in properties, zonal distribution of crosslinking density, viscoelasticity, water content, and pore sizes at micro- and macroscales matrices can be constructed by patterning the hydrogel with IPNs and semi-IPNs.²⁸ These controlled differential structural modifications within the same scaffold are useful for regenerative medicine, which involves co-culturing of more than one type of cells, each requiring matrices with different mechanical properties.

The final approach to regulating the mechanical properties of the collagen gel is through introducing microparticles into collagen gels (Figure 3). For example, incorporating hydrolyzable poly(lactic-co-glycolic acid) (PLGA) microparticles (see product table on page 111) within the collagen gels can increase both the gel's elasticity and rigidity due to the association of PLGA microparticles with the collagen fibrils.²⁹ Interestingly, this approach substantially increases the elastic modulus of the gel without altering the biomolecular diffusivity within the gel. In addition, the PLGA microparticles significantly enhance the deposition of apatite-like minerals within the gels when incubated in simulated body fluid or

encapsulated with mesenchymal stem cells. The favorable osteogenic conditions contributed by the microparticles result in enhanced formation of bone-like tissues.

Summary

This article presents a toolbox of strategies and techniques to customize collagen gels with desired biochemical, mechanical, and transport properties. The highlighted studies serve to greatly advance controllability of structure-property-function of collagen-based materials used for both fundamental and applied bioscience studies relevant to regenerative biology and medicine. Additionally, the underlying principle of material design will be useful in assembling a wide array of biomaterials used for cell culture, drug delivery, and therapies.

References

- (1) Yamauchi, M.; Sricholpech, M. *Essays Biochem.* **2012**, *52*, 113–33.
- (2) Pornprasertsuk, S.; Duarte, W.R.; Mochida, Y.; Yamauchi, M. *J Bone Miner Res.* **2005**, *20*, 81–7.
- (3) Olsen, D.; Yang, C.; Bodo, M.; Chang, R.; Leigh, S.; Baez, J.; Carmichael, D.; Perälä, M.; Hämäläinen, E. R.; Jarvinen, M.; Polarek, J. *Adv Drug Deliv Rev.* **2003**, *55*, 1547–67.
- (4) Merrett, K.; Fagerholm, P.; McLaughlin, C. R.; Dravida, S.; Lagali, N.; Shinozaki, N.; Watsky, M. A.; Munger, R.; Kato, Y.; Li, F.; Marmo, C. J.; Griffith, M. *Invest Ophthalmol Vis Sci.* **2008**, *49*, 3887–94.
- (5) Que, R.; Mohraz, A.; Da Silva, N. A.; Wang, S. W. *Biomacromolecules.* **2014**, *15*, 3540–9.
- (6) Lee, C. R.; Grodzinsky, A. J.; Spector, M. *Biomaterials.* **2001**, *22*, 3145–3154.
- (7) Moshnikova, A. B.; Afanasyev, V. N.; Proussakova, O. V.; Chernyshov, S.; Gogvadze, V.; Beletsky, I. P. *Cellular and Molecular Life Sciences* **2006**, *63*, 229–234.
- (8) Hosseinkhani, H.; Hiraoka, Y.; Li, C. H.; Chen, Y. R.; Yu, D. S.; Hong, P. D.; Ou, K. L. *ACS Chem Neurosci.* **2013**, *4*, 1229–35.
- (9) Shen, Y. H.; Shoichet, M. S.; Radisic, M. *Acta Biomater.* **2008**, *4*, 477–89.
- (10) Zhao, Y.; Zhang, J.; Wang, X.; Chen, B.; Xiao, Z.; Shi, C.; Wei, Z.; Hou, X.; Wang, Q.; Dai, J. *J Controlled Release* **2010**, *141*, 30–7.
- (11) He, Q.; Zhao, Y.; Chen, B.; Xiao, Z.; Zhang, J.; Chen, L.; Chen, W.; Deng, F.; Dai, J. *Acta Biomater.* **2011**, *7*, 1084–93.
- (12) Martin, T. A.; Caliri, S. R.; Williford, P. D.; Harley, B. A.; Bailey, R. C. *Biomaterials* **2011**, *32*, 3949–57.

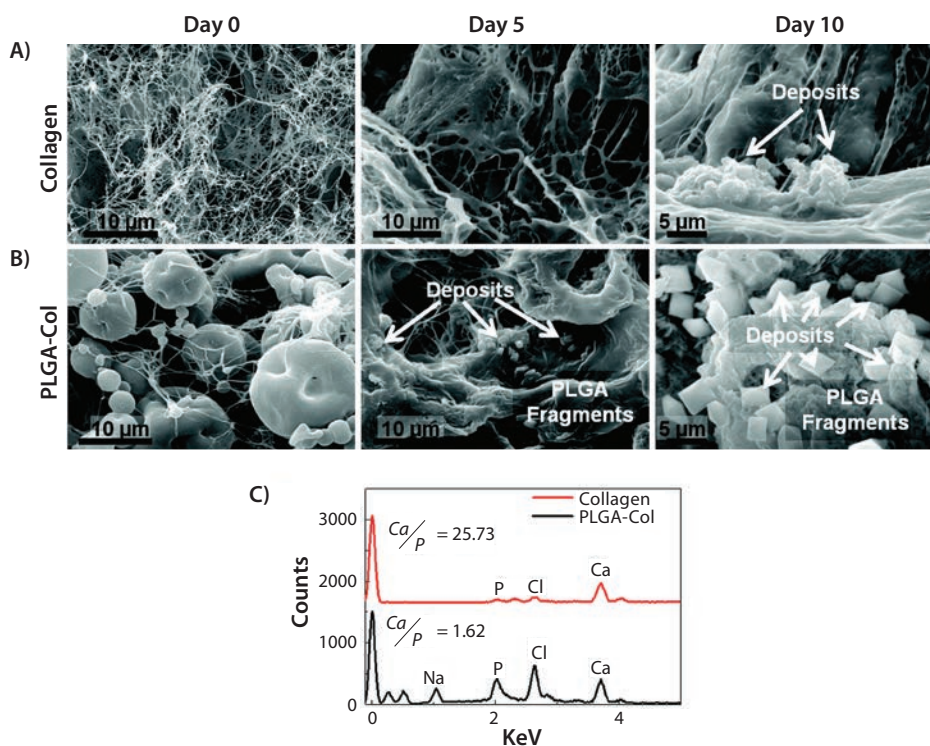


Figure 3. Analysis of minerals formed within MSC-encapsulating hydrogels. **A,B)** SEM images of minerals formed in the MSC-encapsulating collagen **(A)** and PLGA-Col **(B)** hydrogels after 0, 5, and 10 days of incubation in osteogenic differentiation medium. **C)** EDS spectra of minerals formed within the gels. PLGA-Col hydrogels contained 10 mg/mL PLGA particles, while pure collagen gels contained 0 mg/mL. Adapted from Reference 29.

- (13) Alsop, A. T.; Pence, J. C.; Weisgerber, D. W.; Harley, B. A.; Bailey, R. C. *Acta Biomater.* **2014**, *10*, 4715–22.
- (14) Duan, X.; McLaughlin, C.; Griffith, M.; Sheardown, H. *Biomaterials.* **2007**, *28*, 78–88.
- (15) Cao, J.; Xiao, Z.; Jin, W.; Chen, B.; Meng, D.; Ding, W.; Han, S.; Hou, X.; Zhu, T.; Yuan, B.; Wang, J.; Liang, W.; Dai, J. *Biomaterials.* **2013**, *34*, 1302–10.
- (16) Cui, Y.; Lu, C.; Meng, D.; Xiao, Z.; Hou, X.; Ding, W.; Kou, D.; Yao, Y.; Chen, B.; Zhang, Z.; Li, J.; Pan, J.; Dai, J. *Biomaterials.* **2014**, *35*, 7819–27.
- (17) Han, Q.; Sun, W.; Lin, H.; Zhao, W.; Gao, Y.; Zhao, Y.; Chen, B.; Xiao, Z.; Hu, W.; Li, Y.; Yang, B.; Dai, J. *Tissue Eng Part A.* **2009**, *15*, 2927–35.
- (18) Sun, W.; Lin, H.; Xie, H.; Chen, B.; Zhao, W.; Han, Q.; Zhao, Y.; Xiao, Z.; Dai, J. *Growth Factors* **2007**, *25*, 309–18.
- (19) Jia, W.; Tang, H.; Wu, J.; Hou, X.; Chen, B.; Chen, W.; Zhao, Y.; Shi, C.; Zhou, F.; Yu, W.; Huang, S.; Ye, G.; Dai, J. *Biomaterials.* **2015**, *69*, 45–55.
- (20) Shi, C.; Li, Q.; Zhao, Y.; Chen, W.; Chen, B.; Xiao, Z.; Lin, H.; Nie, L.; Wang, D.; Dai, J. *Biomaterials.* **2011**, *32*, 2508–15.
- (21) Choy, A. T.; Leong, K. W.; Chan, B. P. *Acta Biomater.* **2013**, *9*, 4661–72.
- (22) Tiller, J. C.; Bonner, G.; Pan, L. C.; Klibanov, A. M. *Biotechnol Bioeng.* **2001**, *73*, 246–52.
- (23) Liang, Y.; Jeong, J.; DeVolder, R. J.; Cha, C.; Wang, F.; Tong, Y. W.; Kong, H. *Biomaterials.* **2011**, *32*, 9308–15.
- (24) Jeong, J. H.; Liang, Y.; Jang, M.; Cha, C.; Chu, C.; Lee, H.; Jung, W.; Kim, J. W.; Boppert, S. A.; Kong, H. *Tissue Eng Part A.* **2013**, *19*, 1275–84.
- (25) Liang, Y.; Kong, H.; Tong, Y. W. *ACS Macro Lett.* **2013**, *2*, 1077–1081.
- (26) Sosnik, A.; Sefton, M. V. *Biomaterials.* **2005**, *26*, 7425–35.
- (27) Baek, K.; Clay, N. E.; Qin, E.; Sullivan, K.; Kong, H. J. *Eur. Polym. J.* **2015**, doi:10.1016/j.eurpolymj.2015.07.044.
- (28) Suri, S.; Schmidt, C. E. *Acta Biomater.* **2009**, *5*, 2385–97.
- (29) DeVolder, R. J.; Kim, I. W.; Kim, E. S.; Kong, H. *Tissue Eng Part A.* **2012**, *18*, 1642–51.

High-purity Collagen

For more information on these products, visit aldrich.com/natural.

Name	Concentration	Purity (%)	Prod. No.
Bovine Collagen Solution, Type I	3 mg/mL in 0.1 M HCl	≥95	804592-20ML
Bovine Collagen Solution, Type I	6 mg/mL in 0.1 M HCl	≥95	804622-20ML
Bovine Collagen Solution, Acid soluble telocollagen, Type I	6 mg/mL in 0.1 M HCl	≥95	804614-20ML

Other Natural Polymers

Chitosan

For more information on these products, visit aldrich.com/natural.

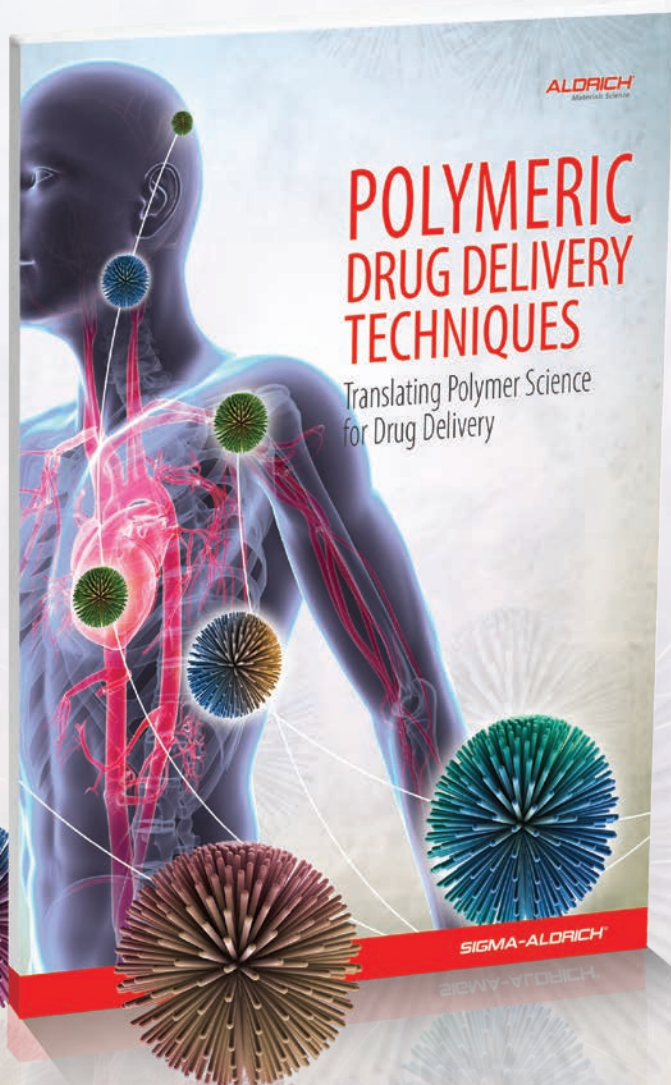
Name	Inherent Viscosity (cP)	Degree Of Deacetylation	Prod. No.
Chitosan	20-300	75-85% deacetylated	448869-50G 448869-250G
	200-800	75-85% deacetylated	448877-50G 448877-250G
	800-2000	>75% deacetylated	419419-50G 419419-250G
Chitosan oligosaccharide lactate	-	> 90% deacetylated	523682-1G 523682-10G

Alginate Acid

For more information on these products, visit aldrich.com/natural.

Name	Inherent Viscosity (cP)	Prod. No.
Alginate acid	15-20	180947-100G 180947-250G 180947-500G

TRANSLATING POLYMER SCIENCE FOR DRUG DELIVERY



A guide to drug delivery solutions using polymers for controlled release, targeted drug delivery and solubility enhancement.

- Step-by-step methods written by drug delivery experts highlighting polymer-based methods to solve the most important drug delivery challenges
- Solutions for:
 - Small molecules
 - Nucleic acids
 - Proteins
- Key technologies:
 - Drug conjugation and PEGylation
 - Biodegradable nanoparticles and micelles
 - RAFT polymeric carriers for ADCs
 - Dendrons
 - Responsive drug delivery systems
 - Polymers for oligonucleotide delivery

Request your copy online at
aldrich.com/ddtechnique